First-report on Mesozoic eclogite-facies metamorphism preceding Barrovian overprint from the western Rhodope (Chalkidiki, northern Greece)

Konstantinos Kydonakis, Evangelos Moulas, Elias Chatzitheodoridis, Dimitrios Kostopoulos, Jean-Pierre Brun

First-report on Mesozoic eclogite-facies metamorphism preceding Barrovian overprint from the western Rhodope (Chalkidiki, northern Greece)

Konstantinos Kydonakis[a], Evangelos Moulas[b,c], Elias Chatzitheodoridis[d], Jean-Pierre Brun[a], Dimitrios Kostopoulos[e]

[a]Géosciences Rennes, UMR 6118CNRS, Université Rennes1, Campus de Beaulieu, 35042 Rennes, France

[b]Institut des sciences de la Terre, Université de Lausanne, 1015 Lausanne, Switzerland

[c]Department of Earth Sciences, ETH Zurich, Sonneggstrasse 5, 8092 Zurich, Switzerland

[d]National Technical University of Athens, School of Mining and Metallurgical Engineering, Department of Geological Sciences, Laboratory of Mineralogy

[e]Faculty of Geology, Dep. of Mineralogy and Petrology, National and Kapodistrian University of Athens, Panepistimioupoli, Zographou, Athens 15784, Greece

Corresponding author: Konstantinos Kydonakis, Géosciences Rennes UMR 6118, Université de Rennes 1, Rennes CEDEX, France (konstantinos.kydonakis@gmail.com)

Highlights

We found eclogite-facies assemblage in a Barrovian complex of northern Greece

The pelitic eclogites re-equilibrated later under amphibolite-facies conditions

Our results suggest subduction of the Barrovian complex prior to the overprint

ABSTRACT

The Chalkidiki block in Northern Greece represents the southwesternmost piece of the ultrahigh-pressure Rhodope and has played an important role in the evolution of the North Aegean. The eastern part of the Chalkidiki block is a basement complex (Vertiskos Unit) that is made largely of Palaeozoic granitoids and clastic sediments metamorphosed during the Mesozoic. This basement is traditionally considered as part of the Rhodopean hanging-wall, an assignment mainly supported by the absence of high-pressure mineral indicators and the presence of a regional medium-pressure/medium-temperature amphibolite-facies Barrovian metamorphic imprint. Toward the west, the basement is juxtaposed with meta-sedimentary (Circum-Rhodope belt) and arc units (Chortiatis Magmatic Suite) that carry evidence of a Mesozoic high-pressure/low-temperature event. In this study, garnet-staurolite-mica schists from the eastern part of the basement were examined by means of micro-textures, mineral chemistry and isochemical phase-diagram sections in the system NCKFMASHMn(Ti) [Na_2O-CaO-K_2O-FeO-MgO-Al_2O_3-SiO_2-H_2O-MnO-(TiO_2)]. The schists represent former Mesozoic sedimentary sequences deposited on the Palaeozoic basement. We document the presence of a relict eclogite-facies mineral assemblage (garnet + chloritoid + phengite + rutile) in an amphibolite-facies matrix composed of garnet + staurolite + phengite ± kyanite. Model results suggest the existence of a high-pressure/medium-temperature metamorphic event (1.9GPa / 520°C) that preceded regional re-equilibration at medium-pressure/medium-temperature conditions (1.2GPa / 620°C). Clearly, the eastern part of the Chalkidiki block (basement complex) retains memory of an as yet unidentified Mesozoic eclogitic metamorphic event that was largely erased by the later Barrovian overprint. In the light of our findings, the basement complex of the Chalkidiki block shares a common tectono-metamorphic evolution with both the high-pressure units to the west, and the high-grade Rhodopean gneisses further to the northeast. Our results are consequential for the

geodynamic reconstruction of the Rhodope since they require participation of the Chalkidiki block to the well-established Mesozoic subduction system.

Keywords: *Aegean, Serbo-Macedonian, garnet-staurolite schists, eclogite, high-pressure low-temperature metapelites, isochemical phase diagrams*

1. Introduction

High-pressure (HP) metamorphic assemblages are commonly overprinted under medium- (MT) or high-temperature (HT) conditions at different stages of the thermal evolution of an orogen. At regional scale, the process responsible for such overprint can be linked to radiogenic heating of a thickened crust, heat produced by viscous dissipation or thermal pulses related to upwelling mantle (e.g., Burg and Gerya, 2005; England and Thompson, 1984; Molnar and England, 1990). A common feature in many mountain belts is the juxtaposition of rocks that underwent high-pressure/low-temperature (HP/LT) metamorphism with rocks that are dominated by medium-pressure/medium-temperature (MP/MT) or medium-pressure/high-temperature (MP/HT) metamorphic assemblages (e.g., Okay, 1989; Whitney et al., 2011). Two scenarios that explain such juxtaposition can be: (i) either all rocks experienced early HP/LT metamorphism but subsequently some of them completely re-equilibrated under MT or HT conditions or (ii) that the juxtaposition occurred during a post-metamorphic stage and thus, is of tectonic nature. Deciphering between the mentioned scenarios can be hard in the absence of any preserved HP relicts from the MP/MT (or MP/HT) rocks.

The Rhodope Metamorphic Province (northern Greece - southern Bulgaria) is a recently established ultrahigh pressure (UHP) metamorphic province (Mposkos and Kostopoulos, 2001; Perraki et al., 2006; Schmidt et al., 2010; see recent review by Burg, 2012). Peak metamorphic conditions and subsequent amphibolite-facies metamorphic overprint are recorded by metapelites that locally contain microdiamond inclusions and by variably retrogressed mafic eclogites (e.g., Liati and Seidel, 1996; Moulas et al., 2013; Mposkos and Kostopoulos, 2001). The southwestern part of the Rhodope Metamorphic Province is exposed at the Chalkidiki Peninsula of northern Greece and has attracted relatively less attention. There, three major units crop out: a) an HP Upper Jurassic magmatic

arc sequence in the west, b) an HP Triassic - Jurassic meta-sedimentary sequence in the middle and c) a Palaeozoic - Lower Mesozoic basement complex that records MP/MT metamorphic conditions in the east. The latter is considered as part of the Rhodopean hanging-wall, an assignment which is supported by the absence of HP relicts and the dominant MP amphibolite-facies regional metamorphic overprint.

In this contribution we study key metapelitic samples from Chalkidiki by means of micro-textures and mineral chemistry. We then compare selected samples (chloritoid-bearing garnet-staurolite-mica schists) to modelled mineral assemblages in the NCKFMASHTiMn (Na_2O-CaO-K_2O-FeO-MgO-Al_2O_3-SiO_2-H_2O-TiO_2-MnO) model system and using isochemical phase-diagram sections we infer the peak metamorphic conditions. This allows us to link, both genetically and temporally, the metamorphic events of the Chalkidiki and define the nature of juxtaposition of the HP units with the MP/MT basement. Our results are consequential for the geodynamic reconstruction of the Rhodope Metamorphic Province since their interpretation requires to re-define the position of the Chalkidiki to better fit into the overall Mesozoic convergence setting.

2. Geological background

2.1 The Hellenides

The Hellenides constitute an integral part of the Alpine-Himalayan mountain chain and are the product of convergence between the stable South European margin and northward-driven Gondwana-derived continental fragments (e.g., Stampfli and Borel, 2002). They are formed by Mesozoic - Cenozoic southwestward piling-up of three continental blocks (namely the Rhodopia, Pelagonia and the External Hellenides) and the closure of two intervening oceanic domains, now forming the Vardar-Axios and Pindos Suture Zones, to the

north and south, respectively (Papanikolaou 2009; and references therein). Seismic tomography illustrates beneath the Hellenides and down to 1600 Km depth a northward-dipping slab, anchored into the lower mantle (Bijwaard et al., 1998). A review of a number of studies (e.g., Jolivet and Brun, 2010; Papanikolaou, 2013; Royden and Papanikolaou, 2011) can summarise the geodynamic evolution of the Hellenides into: (i) a Mesozoic crustal thickening phase followed by (ii) a continuous southward retreat of the subducting Hellenic slab since the Eocene that triggered large-scale extension concomitant with thrusting at the southern part of the Hellenic domain.

2.2 The Rhodope Metamorphic Province (RMP)

The *Rhodope Metamorphic Province*, or simply *Rhodope*, constitutes the hinterland of the Hellenides (northeast Greece - southwest Bulgaria) (Burg et al., 1996; 2012; Krenn et al., 2010; Ricou et al., 1998) (Fig.1a). It can be viewed as a Mesozoic southwestward piling-up, crustal-scale, syn-metamorphic, amphibolite-facies duplex (Burg et al., 1996; Ricou et al., 1998) strongly affected by Cenozoic extension of core complex type (Bonev et al., 2006; Brun and Sokoutis, 2007) and syn- to post-tectonic magmatism (e.g., Kolocotroni and Dixon, 1991; Marchev et al., 2013). The Rhodope is bordered to the north by the Maritza dextral strike-slip fault, to the east by the Middle Eocene to Quaternary Thrace Basin, to the south by the Vardar-Axios - Thermaikos basins which in turn roughly correlate with the Vardar Suture Zone (VSZ) and to the south by the North Aegean Trough. Following Kydonakis et al. (2015), we adopt here a simple threefold division where Rhodope is divided, from northeast to southwest, into three tectonic domains: (i) the *Northern Rhodope Domain* (NRD), (ii) the *Northern* and *Southern Rhodope Core Complexes* (NRCC - SRCC), and (iii) the *Chalkidiki block* (Fig.1a).

To the northeast, within the NRD, typical rocktypes are orthogneisses, mafic eclogites and amphibolites, paragneisses, ultramafics and scarce marble horizons (e.g., Liati and Seidel, 1996; Moulas et al., 2013; Proyer et al., 2008). Although upper amphibolite-facies metamorphic rocks are widespread, many occurrences of variably retrogressed eclogites that preserve evidence of a precursor HP phase have been reported in the literature (e.g. Burg, 2012; Moulas et al., 2013; and references therein). Evidence of UHP conditions is due to the presence of micro-diamond inclusions in metapelites (Mposkos and Kostopoulos, 2001; Perraki et al., 2006; Schmidt et al., 2010) that indicate minimum local pressure of 3.0GPa (for 600^{o}C). Jurassic and Cretaceous zircon metamorphic ages (circa 150 and 75 Ma) from both garnet-kyanite gneisses and amphibolitised eclogites have been reported (Liati et al., 2011; and references therein). Metamorphic conditions for the HP event recorded in mafic rocks are estimated at 1.9GPa / 700^{o}C (Liati and Seidel, 1996) and for the regional amphibolite-facies overprint at 0.7GPa / 720^{o}C (Moulas et al., 2013). Metapelite assemblages record higher pressure for the high-temperature overprint (1.2-1.3GPa / 700-730°C; Krenn et al. 2010).

2.3 The Chalkidiki block

The southwestern part of the Rhodope is the so-called Serbo-Macedonian Massif of Kockel et al. (1971). The term “Massif” has been rejected by many, if not all, workers afterward and the term Serbo-Macedonian Domain should be used instead. Based on the reference map of Kockel and Mollat (1977) it is composed, from west to east, of four units namely the *Chortiatis Magmatic Suite*, the *Circum-Rhodope belt*, the *Vertiskos Unit* (equivalent to Vertiskos Formation/Series) and the *Kerdylion Unit* (equivalent to Kerdylion Formation/Series) (see also Kauffmann et al., 1976; Kockel et al., 1971; 1977). The latter unit that is located below the Kerdylion Detachment shares a common tectono-thermal history

with the SRCC (Brun and Sokoutis, 2007; Himmerkus et al., 2012). The remaining three units define collectively the Chalkidiki block and constitute the hanging-wall of the Kerdylion Detachment, the structure responsible for the exhumation of the SRCC immediately to the east (Fig.1b). During exhumation of the latter, the Chalkidiki block underwent a circa 30^{o} clockwise rotation (Brun and Sokoutis, 2007; and references therein).

The *Vertiskos Unit* is an elongated basement belt with complex tectono-metamorphic history (Burg et al., 1995; Kilias et al., 1999) (Fig.1b). It is a distinct basement fragment that detached from Gondwana and incorporated into the Southern European Arcs by the end of the Palaeozoic (Kydonakis et al., 2014; and references therein). Typical rock types are Silurian - Ordovician granitoids later transformed into orthogneisses (Himmerkus et al., 2009; and our data), paragneisses and thin marble horizons, leucocratic granitic/pegmatitic intrusions, deformed amphibolites, scarce eclogite boudins and serpentinites (Kockel et al., 1971, 1977). Evidence of an early HP episode in the Vertiskos Unit comes from rare eclogite occurrences. For example, Kourou (1991) described eclogite relicts in the cores of amphibolite boudins enclosed in gneisses. Kostopoulos et al. (2000) reported an eclogite lens mantled by trondhjemite enclosed, in turn, in amphibolites near Galarinos village. Korikovsky et al. (1997) studied partially retrograded eclogite lenses within an amphibolite-gneiss metamorphic sequence from the Buchim Block (~15 km SE of Štip, F.Y.R.O.M.). With the exception of a Sm-Nd mineral isochron of 260 ± 49 Ma for the afore-mentioned lenses (mentioned in passing by Korikovsky et al., 1997), the age of the HP event remains unknown and its attribution to Alpine processes can neither be inferred nor excluded. A regional medium-pressure amphibolite-facies event is estimated at 0.45-0.75GPa / 510-580^{o}C from the study of quartz + white mica + biotite + garnet + oligoclase ± staurolite ± kyanite schists (Kilias et al., 1999) and at 0.4GPa / 450-550^{o}C from meta-ultramafics with the assemblage antigorite + Fe-Cr spinel + ilmenite ± chlorite ± talc ± tremolite (Michailidis,

1991). Deformed amphibolites from the basement yield the crucial assemblage amphibole + epidote/zoisite + garnet + quartz + plagioclase ± biotite indicating amphibolite-facies conditions at 0.85GPa / 600^{o}C (our unpublished results). Upper Jurassic - Cretaceous metamorphic ages (^{40}Ar/^{39}Ar, K/Ar and Rb/Sr on micas and amphiboles) have been reported from the basement (e.g., Lips et al., 2000; Papadopoulos and Kilias, 1985; de Wet et al., 1989).

The *Circum-Rhodope belt* is a Triassic - Jurassic meta-sedimentary sequence locally involving Triassic rhyolites and quartzites at the base (see recent review in Meinhold and Kostopoulos, 2013) (Fig.1b). The term Circum-Rhodope belt was originally introduced by Kauffmann et al. (1976) to describe low-grade rocks fringing the basement complex of the Vertiskos Unit to the west, thought of as representing the original Mesozoic stratigraphic cover of the basement. Indeed, Meinhold et al. (2009) reported detrital zircon ages from the base of the meta-sedimentary sequences of the Circum-Rhodope belt and assigned the Vertiskos Unit as their source area. Remnants of garnet-kyanite-staurolite-mica schists toward the eastern part of the Vertiskos Unit have been originally mapped as parts of the Circum-Rhodope belt (Kockel et al., 1977). Some workers interpreted them as separate units and local names where assigned to them (i.e., “Nea Madytos Unit” of Sakellariou and Dürr, 1993; “Bunte Serie” of Papadopoulos and Kilias, 1985). However, their map continuity with the Circum-Rhodope belt further to the west strongly suggests that those sequences are part of the Mesozoic sedimentary cover (Dixon and Dimitriadis, 1984) (Fig.1b). The *Chortiatis Magmatic Suite*, immediately to the west of the Circum-Rhodope belt, is made of intensively deformed acidic and intermediate igneous rocks of Upper Jurassic protolith age (Monod, 1964) (Fig.1b).

Evidence of a HP event from the Circum-Rhodope belt and the Chortiatis Magmatic Suite is found in Asvesta (1992) who reported high-Si phengite from the base of the former

and in Monod (1964) who mentioned “amphiboles which show sometimes a sodic character” from the latter. Michard et al. (1994) also reported the existence of high-Si phengite (3.52 apfu) from basal rhyolitic meta-tuffs of the Circum-Rhodope belt and relict phengite-glaucophane assemblage from the Chortiatis Magmatic Suite. The same authors estimated peak conditions at circa 0.8GPa / 350^{o}C for the HP event. However, a pervasive greenschist-facies overprint seems to have almost completely erased the evidence of this early HP event. We note here that further to the west, lawsonite and Na-amphibole (winchite and barroisite) have been reported from the Paikon Arc (Baroz et al., 1987) which is considered as equivalent to the Chortiatis Magmatic Suite (Anders et al., 2005).

3. Methods / Sampling

3.1 Whole-rock chemistry

Selected key samples were first crushed in a steel jaw crusher and then ground in an agate mortar. The powders were digested using standard lithium metaborate ($LiBO_2$) fusion and acid dissolution techniques and subsequently chemically analysed for major elements by ICP-MS (ACME Labs, Vancouver, Canada).

3.2 Mineral chemistry

Mineral analyses and garnet elemental maps were obtained at ETH Zurich, Switzerland and at Ifremer (Institut français de recherche pour l’expoitation de la mer), Brest, France using a JEOL JXA 8200 and a Cameca SX 100 electron probe, respectively. Both probes were equipped with 5 wavelength dispersive spectrometers operating at an accelerating voltage of 15 kV with a 2 μm beam diameter and 20 nA beam current. Natural

and synthetic materials were used as standards and a CITZAF correction procedure was applied. Back-scattered images were obtained at Université de Rennes1, France and National Technical University of Athens, Greece using a JEOL JSM-7100F Field-Emission Scanning Electron Microscope and a JEOL JSM-6380 Low Vacuum Scanning Electron Microscope, respectively, both operating at an accelerating voltage of 20 kV.

3.3 Phase equilibria thermodynamic modelling

Isochemical phase-diagram sections were calculated using Gibbs free-energy minimisation (Connolly, 2005). Calculations performed in the NCKFMASHMn(Ti) [Na_2O-CaO-K_2O-FeO-MgO-Al_2O_3-SiO_2-H_2O-MnO-(TiO_2)] model system using the solution models given in Table1 and the thermodynamic database of Holland and Powell (1998, revised 2002). Calcium oxide (CaO) present in apatite was subtracted from the total CaO since apatite is not considered in the thermodynamic calculations. The solution model files can be found at http://www.perplex.ethz.ch/ (Perple_X_6.7.0_data_files.zip/solution_models.dat).

3.4 Sampling grid / Strategy

We have selected three key samples for thermodynamic modelling and P-T estimates (Fig.1b). CR4 is a phyllite from the Mesozoic meta-sedimentary cover (Circum-Rhodope belt) that has experienced an early HP imprint. As mentioned before, relict HP minerals are extremely rare along this belt due to later greenschist-facies overprint. Sample CR4 does not contain any HP index mineral and thus, our target is to provide a minimum temperature estimate during the later thermal overprint. Samples SM54 and SM40 are typical garnet-

staurolite schists from the eastern part of the study area and belong to a series of small outcrops embedded in basement rocks (Fig.1b).

4. Petrography

Sample CR4 is a fine-grained quartz-mica phyllite. In the field it has a dominant foliation and a prominent NW-trending crenulation lineation. The main mineral phases are, in decreasing modal amount, quartz, white mica, chlorite, garnet and opaque minerals. A typical crenulation cleavage is developed by differentiation at the limps of the microlithon domains (Fig.2a,b). The microlithons are dominated by quartz and kinked, often chloritised, medium-grained white micas (Figs.2a,b). The cleavage domains are made of fine-grained K-rich white micas or a fine-grained aggregate composed of K-rich white mica, paragonite and chlorite (Fig.2c). Garnet (typically 2-3 mm in diameter) appears heavily replaced by chlorite and is only preserved as small patches within the chlorite mass (Fig.2d). Despite the chlorite alteration, syn-tectonic features are still preserved. Quartz in the microlithon domains has healing features and is recrystallised with sharp grain boundaries and virtually no undulose extinction.

Sample SM54 is a representative garnet-staurolite schist. Major phases are white mica, quartz, chlorite, garnet, staurolite, biotite, and sub-ordinate kyanite. Chloritoid also occurs in small amounts but only as inclusion in garnet. Accessory minerals are rutile (commonly rimmed by ilmenite), apatite, zircon and opaques. Garnet appears with exceptionally large grains measuring up to 1 cm in diameter and is the dominant porphyroblast enveloped by a medium- to fine-grained foliation made of white micas and quartz-rich bands. Shear bands and macroscopically visible spiral garnet indicate top-to-SW sense of shear in hand specimen (Fig.3a). Under the microscope garnet appears euhedral to

subhedral. It contains a relict internal foliation made of aligned quartz, chloritoid, chlorite, margarite, paragonite, phengite and rutile (often rimmed by ilmenite). The internal foliation of the garnet is in continuity with the external one implying syn-tectonic garnet growth (Figs.4a). The matrix foliation is made of quartz, phengite and intergrowths of phengite/paragonite (Fig.4b). Staurolite shows similar syn-tectonic features and contains quartz, biotite and chlorite as inclusions (Figs.4c,d). The internal foliation in garnet and staurolite is virtually linear/flat while the external one is heavily folded. Extremely rare kyanite crystals are observed exclusively in the matrix. Rutile exists also in the matrix where it is rimmed by ilmenite. Hematite occurs in trace amounts in the matrix and in association with chlorite in late cracks.

Sample SM40 is similar to SM54 in terms of texture, mineralogy and deformation pattern. Major phases are white mica, quartz, garnet, chlorite, staurolite and rutile. Accessory minerals are monazite, zircon, and rarely ilmenite and allanite. The matrix is made of phengite, paragonite, rutile and quartz. Garnet appears as euhedral to subhedral grains measuring up to 1.5 cm in diameter (Fig.3b) and contains white mica, rutile, ilmenite, chlorite, rare pyrite and an impressive amount of tourmaline as aligned inclusions. Staurolite is relatively rare compared to SM54 but appears in larger crystals. As in sample SM54, both garnet and staurolite show syn-tectonic features. Rutile also appears as large porphyroblasts in the matrix often surrounded by chlorite. Contrary to SM54, no chloritoid was found in this sample.

5. Mineral chemistry

A mineralogical assemblage table as well as the bulk composition of each studied sample are given in Table2. Selected mineral analyses from the phyllite and the garnet-

staurolite schists are given in Table3. An overview of the micas and garnet compositions is shown in Fig.5 and Fig.6, respectively.

CR4

The foliation is made of locally chloritised phengite/paragonite intergrowths. The Si content of the K-rich mica from the matrix ranges from 3.1 to 3.25 apfu and contains up to 2.4 wt% Na_2O. Paragonite from the matrix has Na/(Na+K) ratio (atoms per formula unit - apfu) around 0.9 and contains small amount of Ca (less than 0.1 apfu). No systematic chemical variation between the large (microlithon domains) and the smaller (crenulation domains) mica grains was observed. Quartz and iron oxides are also common in the matrix. Garnet is extremely rare as it has been almost entirely replaced by chlorite. Garnet composition is between $Alm_{67}Grs_{23}Sps_{6}Pyr_{4}$ and $Alm_{60}Grs_{25}Sps_{12}Pyr_{3}$. The maximum measured Mg# (Mg/[Mg+Fe], apfu) of the chlorite that replaces garnet is 0.38.

SM54

White micas show a range of compositions. Potassium-rich white mica is dominant in the matrix and along with paragonite form the main foliation of the rock. The Si content of the K-rich mica ranges from 3.08 to 3.25 apfu. White micas that are included in the garnet have more paragonite-rich and margarite-rich compositions. Paragonite and margarite inclusions in the garnet show fine-grained intergrowths (Fig.4a) compared to the more coarse-grained intergrowths of matrix K-rich white mica and paragonite (Fig.4b). Paragonite inclusions have Na/Na+K (apfu) ratio up to 0.94 and contain small amount of Ca (less than 0.13 apfu). Margarite contains between 0.17 and 0.39 apfu Na content. Chloritoid is Fe-rich (Mg# between 0.18 and 0.22 apfu) and appears exclusively as inclusion in garnet parallel to an internal, virtually linear/flat, foliation in relation with margarite, paragonite and rutile (sometimes surrounded by ilmenite) (Fig.4a). Annite-rich biotite is dominant in the matrix

(Mg# between 0.32 and 0.47) and phlogopite-rich biotite (Mg# up to 0.65) is found as inclusion in staurolite (Fig.4d). Similar to biotite, matrix chlorite has lower Mg# (0.35-0.48) compared to the chlorite crystals included in staurolite (0.6). The Al content of biotite varies between 2.5 and 3 apfu. Garnet shows zoning in major elements and its composition ranges from $Alm_{67}Grs_{18}Sps_{11}Pyr_4$ to $Alm_{79}Grs_7Sps_0Pyr_{14}$, from core to rim, characteristic, characteristic for growth during temperature increase (e.g., Harris et al., 2004) (Fig.7). Staurolite Mg# ranges from 0.18 to 0.23.

SM40

Potassium-rich white mica is dominant in the matrix and its composition has up to 3.25 apfu Si and up to 0.24 apfu Na contents. Paragonite is less abundant with Na/Na+K ratio up to 0.9 and it contains less than 1 wt% CaO (0.04 apfu). Chlorite shows a narrow range of compositions with Mg# between 0.45 and 0.51. Garnet has composition similar to that of SM54 and displays zoning in major elements with $Alm_{65}Grs_{20}Sps_{11}Pyr_4$ cores and $Alm_{80}Grs_9Sps_0Pyr_{11}$ rims. As mentioned before, tourmaline is abundant as inclusion in the garnet but it has never been observed elsewhere. It belongs to the dravite series and it contains about 3 wt% Na_2O and less than 1 wt% CaO. Staurolite Mg# ranges from 0.19 to 0.22.

6. Isochemical phase-diagram P-T sections

6.1 Garnet-bearing phyllite

An isochemical phase-diagram section for the sample CR4 has been calculated for the range 0.4-1.6GPa and 350-650^{o}C (Fig.8). Due to the absence of rutile, titanite and ilmenite this particular sample composition was modelled in the NCKFMASHMn (i.e., TiO_2 was not

considered). For the calculations, total Fe was assumed to be Fe^{+2} and water was taken in excess using the CORK equation of state (EOS) of Holland and Powell (1998). Quadri-variant fields dominate over the calculated P-T area. Penta-variant fields are common at low pressure and low temperature whereas few tri-variant fields are mostly related to the garnet-in and biotite-in reactions. Glaucophane and lawsonite are the Na- and Ca-bearing phases at HP/LT conditions. Potassium- (Wmca1) and Na-white micas (Wmca2) are present in the studied P-T range and they reduce to a single white mica only at T > 600^{o}C for low pressure conditions. Chloritoid is stable above 1.1GPa for T < 550^{o}C. Garnet and biotite are stable at T > 500^{o}C and T > 550^{o}C, respectively. Calculations on the mineral volume and Mg# as well as the garnet end-member molar amounts are given in AppendixA1.

The only evidence for HP metamorphism in the sample can be considered the Si content of the white micas that reaches up to 3.25 apfu. According to the results of the phase-diagram section, this is attained at maximum pressure of 1.5GPa (at arbitrarily-chosen temperature of 350^{o}C; see also AppendixA1). At these conditions, chloritoid, glaucophane and lawsonite participates with 3, 2 and less than 1% in the volume of the rock, respectively, and can be considered as easy to be consumed at a later stage. In the presence of Mn in the system, garnet can be stable at lower temperature than those predicted for Mn-free systems (Symmes and Ferry, 1992; White et al., 2014). Therefore the garnet isograd in the NCKFMASHMn is an excellent marker for the minimum temperature attained during the overprint. As described in the petrography section, garnet is extensively replaced by chlorite (Fig.2d) and this can potentially shift garnet's composition (particularly the X_{Fe} and X_{Mg} components) during replacement. As a result, the measured garnet's compositional isopleths do not cross at a narrow area. The Mn content of garnet suggests that the temperature reached 550^{o}C and this is accordance with the maximum measured chlorite Mg# (Fig.8). Based on the intersection of the spessartine content of the garnet and the Mg# of the chlorite that replaces

garnet, the conditions can be roughly constrained as P < 0.8GPa and T = 550^{O}C (Fig.8). Biotite is stable at T > 550^{o}C (in small amounts, see AppendixA1) but was not observed in the rock. Thus, although no reliable pressure estimation can be made, the temperature during the retrogression more likely reached 550^{o}C for P < 0.8GPa.

6.2 Garnet-staurolite schists

Isochemical phase-diagram sections have been calculated in the range 0.4-2.4GPa and 450-750^{o}C for the garnet-staurolite schists (samples SM54 and SM40) in the NCKFMASHMnTi model system. For the calculations, total Fe was assumed to be Fe^{+2}. This is supported by the absence of hematite from the main porphyroblasts (garnet and staurolite). On the contrary, rare hematite is found in the matrix foliation and thus, it is safe to conclude that oxidisation occurred at the post-peak stage of the rock evolution. Water was assumed as a phase in excess using the CORK EOS after Holland and Powell (1998). For reasons of clarity, we will thoroughly describe the results of SM54. Those of the SM40 are given in AppendicesA2, A3 and A4. We note that very similar phase-diagram sections were calculated for both samples and the inferred P-T paths are in general agreement.

The topology of the phase-diagram section for sample SM54 is shown in Fig.9. Quadri-variant fields dominate over the entire P-T. Tri-variant fields are dominant at medium-to high-pressure and low-temperature conditions. The P-T phase-diagram section predicts the existence of glaucophane and lawsonite as the Na- and Ca-bearing phases at HP/LT conditions. Potassium- (Wmca1) and Na-white micas (Wmca2) are present in the studied P-T range and they reduce to a single white mica only at HT and P < 1.0GPa conditions. Garnet is stable at T > 500^{o}C. Chloritoid is restricted at P > 0.8GPa and it disappears for T > 600^{o}C. Biotite is stable at T > 520^{o}C and both with staurolite are stable at

P < 1.3GPa. Calculations on the mineral volume and Mg# as well as the garnet end-member molar amounts are given in AppendixA5.

Based on textural observations, a first mineral assemblage is characterised by the co-existence of garnet, chloritoid, white mica and rutile (Fig.4a). The relative large size of the garnet crystals (cm scale) and the temperature estimate that is below 650^{o}C (see section below) implies that garnet's growth composition has not been significantly changed by diffusion (e.g., Caddick et al., 2010). This allow us to use composition isopleths to infer the metamorphic P-T history. Garnet core isopleths and chloritoid Mg# (0.18 - 0.22) cross at 1.8-2.0GPa / 520^{o}C (Fig.9). This in agreement with the maximum measured Si content in phengite which also constrains the pressure to a maximum of 2GPa. Based on the calculated P-T section, this first metamorphic assemblage is located within a tri-variant field that also includes lawsonite and/or glaucophane as Ca- and Na-bearing phases (Fig.9). The modal amount is less than 1% for the lawsonite and less than 8% for the glaucophane and thus, it is reasonable to assume that if ever co-existed with chloritoid at the first stage, they were subsequently consumed at a later stage of the evolution of the rock (c.f. Cruciani et al., 2013). Besides, both Ca- and Na-white micas are seen in coexistence with chloritoid inclusion in garnet and may represent phases after former lawsonite and glaucophane (Fig.4a). The garnet rim composition isopleths cross at 1.5GPa / 570^{o}C, in close proximity to the chloritoid-out reaction. We note that chloritoid is found solely as inclusion in garnet, both in its core and rim. Thus, a heating decompression path within the stability field of chloritoid with increasing garnet volume can be drawn (Fig.9). The peak thermal overprint is deduced from the co-existence of staurolite (Mg# 0.18 - 0.23 apfu), garnet, biotite (maximum Mg# 0.65 apfu as inclusion in staurolite), chlorite (Mg# 0.6 apfu as inclusion in staurolite) and scarce kyanite. The inferred conditions for that stage are constrained at 1.0 - 1.3GPa and 600 - 640^{o}C (Fig.9). Matrix biotite and chlorite record lower Mg# compared to that as inclusion in

staurolite, compatible with the P-T section predictions (Fig.9, AppendixA5) and thus we can infer that both biotite and chlorite record further cooling/decompression metamorphic conditions.

7. Discussion

7.1 Revised P-T path of the garnet-staurolite schists: Barrovian path revisited

The basement complex of the Chalkidiki block has long been considered as showing exclusively a Barrovian MP amphibolite-facies peak metamorphic conditions and as such it has been traditionally considered as part of the Mesozoic Rhodopean hanging-wall. This is supported by i) the predominance of garnet-staurolite schists (typical of amphibolite-facies conditions) that are quite often intercalated within orthogneisses and ii) the lack of any, reliable, evidence for a Mesozoic HP event. In addition, detrital garnet and staurolite are commonly found in recent sedimentary basins sourced from the basement (Georgiadis, 2006) attributing a regional character to the amphibolite-facies overprint.

We have chosen here to study key garnet-staurolite schists (Fig.3) exposed as thin slivers toward the eastern part of the basement to investigate the hypothesis of a preceding HP event of Alpine age before the regional amphibolite-facies overprint (Fig.1b). The schists belong to the Triassic - Jurassic meta-sedimentary cover (Dixon and Dimitriadis, 1984; Kockel and Mollat, 1977; Kockel et al., 1977) and therefore they are excellent candidates to record Alpine tectono-metamorphic events. Similar schists have been studied by Papadopoulos and Kilias (1985) and Sakellariou and Dürr (1993) who identified the mineral assemblage of garnet and staurolite as crucial for the estimation of peak metamorphic

conditions of the area. The previous authors also recognised the existence of kyanite and chloritoid in these rocks but their significance have not been clearly highlighted.

Since the early petrogenetic grids that incorporated thermodynamic data in the simple system KFMASH (K_2O-FeO-MgO-Al_2O_3-SiO_2-H_2O) for pelitic schists, it is known that chloritoid can co-exist with garnet at MP to HP and LT to MT conditions whereas staurolite has a narrow stability field at MP/MT conditions (e.g., Powell and Holland, 1990; Spear and Cheney, 1989; Wei and Powell, 2003). Kyanite is predicted to be present with garnet + chloritoid at eclogite-facies conditions for Al-rich/Mg-poor bulk compositions but is restricted to the higher temperature for decreasing Al content (Wei and Powell, 2003). Indeed garnet + chloritoid assemblage (often co-existing with kyanite, phengite and rutile) has been found in eclogite-facies metapelites from the Alps (e.g., Smye et al., 2010), the Carpathians (e.g., Negulescu et al., 2009), Norway (e.g., Hacker et al., 2003) and Sardinia (Cruciani et al., 2013).

Based on micro-textures, we show that the eclogite-facies garnet + chloritoid + phengite + rutile assemblage precedes the amphibolite-facies garnet + staurolite ± kyanite assemblage (Fig.4). Using phase-diagram sections and mineral chemistry (Figs.5, 6, 7) and with reference to the results of SM54, we inferred early HP conditions at 1.8-2.0GPa / 520^{o}C and subsequent re-equilibration at 1.0-1.3GPa / 600-640^{o}C (Fig.9). Thus, the garnet-staurolite schists carry evidence of a preceding HP event in the eclogite-facies (close to blueschist/eclogite-facies transition) before the regional amphibolite-facies overprint. Based on their protolith age, the HP event is essentially of Mesozoic age. This has an important consequence and necessitates the re-consideration of the regional evolution of the Chalkidiki (see next paragraph).

7.2 Metamorphic evolution of the southwestern Rhodope Metamorphic Province

The Chalkidiki block of northern Greece is the southwestern part of the Rhodope Metamorphic Province and thus, an important element of the latter (Fig.1). There the cover and arc units that are exposed to the west and carry evidence for a HP event are in contact with a basement complex that experienced MP/MT metamorphic conditions (Fig.1b). At a first glance, such juxtaposition seems to impose the existence of a strong discontinuity between the HP units, to the west, and the MP/MT rock units lying to the east. However, as we exemplified here, there is also a preceding HP eclogite-facies event from the basement that was followed by thermal re-equilibration under MP/MT conditions.

At the scale of the whole Chalkidiki block there is a gradient in the metamorphic conditions: from east to the west, they decrease from eclogite-facies (and subsequent amphibolite-facies overprint) to blueschist-facies (and greenschist/lower amphibolite-facies overprint). In detail, according to Michard et al. (1994) peak pressure to the west is of the order of 0.8GPa and based on our results (inferred only from the silica content of white micas), the maximum pressure may have reached 1.5GPa (for arbitrarily chosen temperature of 350^{o}C) (Fig.8). However, our robust estimation for the easternmost part is between 1.8 and 2.0GPa (Fig.9). The same holds true for the temperature variation. According to Michard et al. (1994) the temperature at the peak pressure event was of the order of 350^{o}C for the western part and based on our calculations, the MT overprint reached at least 550^{o}C (Fig.8). However, the MT overprint to the east, was in the order of 650^{o}C (Fig.9).

The discovery of an early HP Alpine event from the MP/MT basement imposes a model that involves common early metamorphic history for both the basement and the HP cover/arc units further to the west. Despite the late variable degree of overprint of the basement and its cover, we argue that their NW-SE-trending contact should not be considered

as an important geological discontinuity (Fig.1b). It is definitely of tectonic origin but both foot-wall and hanging-wall rocks experienced the same metamorphic event reaching, though, different metamorphic conditions.

7.3 Mesozoic metamorphic gradient of the Rhodope Metamorphic Province

As briefly described in the introduction, the Rhodope Metamorphic Province forms the hinterland of the Hellenic Orogen. Following a Jurassic - Cretaceous piling-up phase (Burg et al., 1995; 1996; Ricou et al., 1998), the Tertiary collapse of the Hellenic Orogen resulted in large-scale extension of core complex type and exhumation of migmatitic gneiss domes that dismembered the Rhodopean gneiss imbricates (Brun and Sokoutis, 2007). Block-type behaviour is shown by the NRD to the northeast, and the Chalkidiki block to the southwest, which were separated during the Eocene - Oligocene exhumation of the SRCC (Brun and Sokoutis, 2007) (Fig.1). In other words, restoring the pre-collapse geometry of the Rhodope, thus virtually closing the SRCC, would bring the NRD and the Chalkidiki block in close proximity (see also Kydonakis et al., 2015). It can be further stressed that due to their present-day position the Chalkidiki block occupied, after restoring the pre-collapse geometry, a position immediately south of the NRD. Based on the fact that the Mesozoic convergence occurred in a northward subduction regime, the attained metamorphic conditions are expected to increase northward.

In Fig.10, we compiled the available P-T estimates for the Chalkidiki block (western and eastern parts) and selected reliable estimates for the central and western parts of the NRD. It can be concluded that the metamorphic gradient inferred before for the Chalkidiki block (between its western and eastern parts), can now be expanded to include also the NRD where higher peak-pressure and peak-temperature during decompression is recorded (Fig.10).

This is also in line with the discovery of micro-diamonds from the NRD (Mposkos and Kostopoulos, 2001; Perraki et al., 2006; Schmidt et al., 2010) that implies higher metamorphic conditions toward the northeast. The timing for the peak pressure event is rather unknown for the Chalkidiki block but it is (pre-)Upper Jurassic for the NRD (Liati et al., 2011; and references therein). Subsequent re-equilibration at peak temperature conditions is confined at Cretaceous for both the Chalkidiki block (e.g., Lips et al., 2000; Papadopoulos and Kilias, 1985; de Wet et al., 1989; and our unpublished data) and the NRD (e.g., Bosse et al., 2010; Didier et al., 2014; Krenn et al., 2010; Liati et al., 2011).

We therefore argue that the NRD and the Chalkidiki block participated into the same Mesozoic convergence as part of the same down-going plate along a northward subduction. Both domains recorded early, possibly (pre-)Upper Jurassic, eclogite-facies metamorphic conditions and subsequent Cretaceous re-equilibration at amphibolite-facies conditions. The prevailed metamorphic conditions were different between the domains, both during the peak-pressure and peak-temperature stages, implying the existence of a metamorphic gradient that coincides with increasing metamorphic grade toward the northeast.

8. Conclusions

In this contribution we studied key chloritoid-bearing garnet-staurolite-mica schists (Fig.3) from the eastern part of the basement of the Chalkidiki block (northern Greece) (Fig.1b). The schists represent former Mesozoic sedimentary sequences deposited on a Palaeozoic basement which was prior considered to have experienced exclusively Barrovian MP amphibolite-facies metamorphism of Alpine age. Based on micro-textures, we documented a relict eclogite-facies mineral assemblage (garnet + chloritoid + phengite + rutile) in an amphibolite-facies matrix composed of garnet + staurolite + phengite ± kyanite

(Fig.4). Using mineral chemistry and isochemical phase-diagram sections in the system NCKFMASHMnTi we inferred early HP conditions at 1.8-2.0GPa / 520^{o}C and subsequent re-equilibration at 1.0-1.3GPa / 600-640^{o}C (Fig.9). This finding supports the idea that the basement complex of the Chalkidiki block retains memory of an as yet unidentified Mesozoic eclogite-facies metamorphic event that was largely erased by the Barrovian overprint. At the scale of the Chalkidiki we inferred a gradient in the metamorphic conditions: from blueschist-facies to the west to eclogite-facies toward the east.

In the light of this finding we are able to incorporate the Chalkidiki block into the Mesozoic convergence setting of the Rhodope. The Chalkidiki block and the high-grade Rhodopean gneisses, exposed further to the northeast, participated into the same Mesozoic convergence as part of a northward down-going plate prior to their exhumation and incorporation into the upper plate. Both domains experienced similar metamorphic conditions - yet of varying intensity - that include an early eclogite-facies metamorphic event and subsequent retrogression at MP/MT (or MP/HT) conditions during the Cretaceous. The recorded metamorphic conditions increase northward, i.e., from the Chalkidiki block to the Northern Rhodope Domain, compatible with the well-established northward-dipping Jurassic - Cretaceous subduction.

ACKNOWLEDGEMENTS

This work was funded by the European Union FP7 Marie Curie ITN “TOPOMOD” contract 264517. E.M. acknowledges the ERC starting grant (335577) and the University of Lausanne for financial support. Jean-Pierre Burg and Lucie Tajčmanová are acknowledged for access to the EPMA facility in the ETH Zurich. The comments received by Gabriele Cruciani and an

anonymous reviewer materially helped to improve the original manuscript and are greatly appreciated. Marco Scambelluri is greatly acknowledged for editorial handling.

REFERENCES

Anders, B., Reischmann, T., Poller, U., Kostopoulos, D., 2005. Age and origin of granitic rocks of the eastern Vardar Zone, Greece: new constraints on the evolution of the Internal Hellenides. Journal of the Geological Society, London 162, 857 - 870.

Asvesta, A., 1992. Magmatism and associated sedimentation during the first stage of the opening of the Vardar oceanic basin in Triassic times (in greek with english abstract). Ph.D. thesis, University of Thessaloniki, Greece.

Auzanneau, E., Schmidt, M., Vielzeuf, D., Connolly, J. A. D., 2010. Titanium in phengite: a geobarometer for high temperature eclogites. Contributions to Mineralogy and Petrology 159(1), 1 - 24.

Baroz, F., Bebien, J., Ikenne, M., 1987. An example of high-pressure low-temperature metamorphic rocks from an island-arc: the Paikon Series (Innermost Hellenides, Greece). Journal of Metamorphic Geology 5(4), 509 - 527.

Bijwaard, H., Spakman, W., Engdahl, E. R., 1998. Closing the gap between regional and global travel time tomography. Journal of Geophysical Research: Solid Earth 103(B12), 30055 - 30078.

Bonev, N., Burg, J.-P., Ivanov, Z., 2006. Mesozoic-Tertiary structural evolution of an extensional gneiss dome - the Kesebir-Kardamos dome, eastern Rhodope (Bulgaria-Greece). International Journal of Earth Sciences (Geologische Rundschau) 95(2), 318 - 340.

Bosse, V., Cherneva, Z., Gautier, P., Gerdjikov, I., 2010. Two partial melting events as recorded by the U-Th-Pb chronometer in monazite: LA-ICPMS in situ dating in metapelites from the Bulgarian Central Rhodopes. Geologica Balcanica 39(1 - 2), 51 - 52.

Brun, J.-P., Sokoutis, D., 2007. Kinematics of the Southern Rhodope Core Complex (North Greece). International Journal of Earth Sciences (Geologische Rundschau) 96(6), 1079 - 1099.

Burg, J.-P., 2012. Rhodope: From Mesozoic convergence to Cenozoic extension. Review of petro-structural data in the geochronological frame. Journal of the Virtual Explorer 42(1).

Burg, J.-P., Gerya, T. V., 2005. The role of viscous heating in Barrovian metamorphism of collisional orogens: thermomechanical models and application to the Lepontine Dome in the Central Alps. Journal of Metamorphic Geology 23(2), 75 - 95.

Burg, J.-P., Godfriaux, I., Ricou, L.-E., 1995. Extension of the Mesozoic Rhodope thrust units in the Vertiskos-Kerdilion Massifs. Comptes Rendus de l'Académie des Sciences, Paris 320(IIa), 889 - 896.

Burg, J.-P., Ricou, L.-E., Ivanov, Z., Godfriaux, I., Dimov, D., Klain, L., 1996. Synmetamorphic nappe complex in the Rhodope Massif. Structure and kinematics. Terra Nova 8(1), 6 - 15.

Caddick, M., Konopásek, J., Thompson, A., 2010. Preservation of Garnet Growth Zoning and the Duration of Prograde Metamorphism. Journal of Petrology 51(11), 2327 - 2347.

Coggon, R., Holland, T., 2002. Mixing properties of phengitic micas and revised garnet-phengite thermobarometers. Journal of Metamorphic Geology 20(7), 683 - 696.

Connolly, J. A., 2005. Computation of phase equilibria by linear programming: A tool for geodynamic modeling and its application to subduction zone decarbonation. Earth and Planetary Science Letters 236(1 - 2), 524 - 541.

Cruciani, G., Franceschelli, M., Massonne, H.-J., Carosi, R., Montomoli, C., 2013. Pressure-temperature and deformational evolution of high-pressure metapelites from Variscan NE Sardinia, Italy. Lithos 175 - 176, 272 - 284.

de Wet, A. P., Miller, J. A., Bickle, M. J., Chapman, H. J., 1989. Geology and geochronology of the Arnea, Sithonia and Ouranopolis intrusions, Chalkidiki Peninsula, northern Greece. Tectonophysics 161(1 - 2), 65 - 79.

Didier, A., Bosse, V., Cherneva, Z., Gautier, P., Georgieva, M., Paquette, J. L., Gerdjikov, I., 2014. Syn-deformation fluid-assisted growth of monazite during renewed highgrade metamorphism in metapelites of the Central Rhodope (Bulgaria, Greece). Chemical Geology 381, 206 - 222.

Diener, J. F. A., Powell, R., 2012. Revised activity-composition models for clinopyroxene and amphibole. Journal of Metamorphic Geology 30(2), 131 - 142.

Dixon, J. E., Dimitriadis, S., 1984. Metamorphosed ophiolitic rocks from the SerboMacedonian Massif, near Lake Volvi, North-east Greece. Geological Society, London, Special Publications 17, 603 - 618.

England, P. C., Thompson, A. B., 1984. Pressure-Temperature-Time Paths of Regional metamorphism I. Heat Transfer during the Evolution of Regions of Thickened Continental Crust. Journal of Petrology 25(4), 894 - 928.

Fuhrman, M. L., Lindsley, D. H., 1988. Ternary-feldspar modeling and thermometry. American Mineralogist 71(3 - 4), 201 - 215.

Ganguly, J., Cheng, W., Tirone, M., 1996. Thermodynamics of aluminosilicate garnet solid solution: new experimental data, an optimized model, and thermometric applications. Contributions to Mineralogy and Petrology 126(1 - 2), 137 - 151.

Georgiadis, I., 2006. Petrological and geochemical study of Quaternary clastic sediments from the Cherso basin (in greek), Master's thesis, University of Thessaloniki, Greece.

Hacker, B. R., Andersen, T. B., Root, D. B., Mehl, L., Mattinson, J. M., Wooden, J. L., 2003. Exhumation of high-pressure rocks beneath the Solund Basin, Western Gneiss Region of Norway. Journal of Metamorphic Geology 21(6), 613 - 629.

Harris, N. B. W., Caddick, M., Kosler, J., Goswami, S., Vance, D., Tindle, A. G., 2004. The pressure-temperature-time path of migmatites from the Sikkim Himalaya. Journal of Metamorphic Geology, 22(3) 249 - 264.

Himmerkus, F., Reischmann, T., Kostopoulos, D., 2009. Serbo-Macedonian revisited: A Silurian basement terrane from northern Gondwana in the Internal Hellenides, Greece. Tectonophysics 473(1 - 2), 20 - 35.

Himmerkus, F., Zachariadis, P., Reischmann, T., Kostopoulos, D., 2012. The basement of the Mount Athos peninsula, northern Greece: insights from geochemistry and zircon ages. International Journal of Earth Sciences (Geologische Rundschau) 101(6), 1467 - 1485.

Holland, T., Powell, R., 1998. An internally consistent thermodynamic data set for phases of petrological interest. Journal of Metamorphic Geology 16(3), 309 - 343.

Holland, T., Baker, J., Powell, R., 1998. Mixing properties and activity-composition relationships of chlorites in the system Mgo-FeO-Al2O3-SiO2-H2O. European Journal of Mineralogy 10(3), 395 - 406.

Jolivet, L., Brun, J.-P., 2010. Cenozoic geodynamic evolution of the Aegean. International Journal of Earth Sciences (Geologische Rundschau) 99(1), 109 - 138.

Kauffmann, G., Kockel, F., Mollat, H., 1976. Notes on the stratigraphic and paleogeographic position of the Svoula Formation in the Innermost Zone of the Hellenides (Northern Greece). Bulletin de la Société Géologique de France 7(2), 225 - 230.

Kilias, A., Falalakis, G., Mountrakis, D., 1999. Cretaceous-Tertiary structures and kinematics of the Serbomacedonian metamorphic rocks and their relation to the exhumation of the Hellenic hinterland (Macedonia, Greece). International Journal of Earth Sciences (Geologische Rundschau) 88(3), 513 - 531.

Kockel, F., Mollat, H., 1977. Geological map of the Chalkidiki peninsula and adjacent areas (Greece), Scale 1:100000. Bundesanstalt für Geowissenschaften und Rohstoffe, Hannover.

Kockel, F., Mollat, H., Walther, H. W., 1971. Geologie des Serbe-Mazedonischen Massivs und seines mesozoischen Rahmens (Nordgriechenland). Geologisches Jahrbuch 89(1), 529 - 551.

Kockel, F., Mollat, H., Walther, H., 1977. Erlauterungen zur Geologischen Karte der Chalkidiki und angrenzender Gebiete. Bundesanstalt für Geowissenschaften und Rohstoffe, Hannover, 119 pp.

Kolocotroni, C., Dixon, J. E., 1991. The origin and emplacement of the Vrondou granite, Serres, NE Greece. Bulletin of the Geological Society of Greece XXV(1), 469 - 483.

Korikovsky, S. P., Mirčovski, V., Zakariadze, G. S., 1997. Metamorphic Evolution and the Composition of the Protolith of Plagioclase-bearing Eclogite-Amphibolites of the Buchhn Block of the Serbo-Macedonian Massif, Macedonia. Petrology 5(6), 596 - 613.

Kostopoulos, D., Ioannidis, N., Sklavounos, S., 2000. A New Occurrence of Ultrahigh-Pressure Metamorphism, Central Macedonia, Northern Greece: Evidence from Graphitized Diamonds? International Geology Review 42(6), 545 - 554.

Kourou, A. N., 1991. Lithology, tectonic, geochemistry and metamorphism in the western part of the Vertiskos group. The area NE from the lake Agios Vasilios, northern Greece (in greek), Ph.D. thesis, University of Thessaloniki, Greece.

Krenn, K., Bauer, C., Proyer, A., Klötzli, U., Hoinkes, G., 2010. Tectonometamorphic evolution of the Rhodope orogen. Tectonics 29, TC4001.

Krohe, A., Mposkos, E., 2002. Multiple generations of extensional detachments in the Rhodope Mountains (northern Greece): evidence of episodic exhumation of high-pressure rocks. Geological Society, London, Special Publications 204, 151 - 178.

Kydonakis, K., Brun, J.-P., Sokoutis, D., 2015. North Aegean core complexes, the gravity spreading of a thrust wedge. Journal of Geophysical Research: Solid Earth, accepted.

Kydonakis, K., Kostopoulos, D., Poujol, M., Brun, J.-P., Papanikolaou, D., Paquette, J.L., 2014. The dispersal of the Gondwana Super-fan System in the eastern Mediterranean: New insights from detrital zircon geochronology. Gondwana Research 25(25), 1230 - 1241.

Liati, A., Seidel, E., 1996. Metamorphic evolution and geochemistry of kyanite eclogites in central Rhodope, northern Greece. Contributions to Mineralogy and Petrology 123(3), 293 - 307.

Liati, A., Gebauer, D., Fanning, C. M., 2011. Ultrahigh-Pressure Metamorphism: 25 Years After the Discovery of Coesite and Diamond, chap. Geochronology of the Alpine UHP Rhodope Zone: A Review of Isotopic Ages and Constraints on the Geodynamic Evolution, pp. 295 - 324, Elsevier Inc.

Lips, A. L. W., White, S. H., Wijbrans, J. R., 2000. Middle-Late Alpine thermotectonic evolution of the southern Rhodope Massif, Greece. Geodinamica Acta 13, 281 - 292.

Marchev, P., Georgiev, S., Raicheva, R., Peytcheva, I., von Quadt, A., Ovtcharova, M., Bonev, N., 2013. Adakitic magmatism in post-collisional setting: An example from the Early-Middle Eocene Magmatic Belt in Southern Bulgaria and Northern Greece. Lithos 180 - 181, 159 - 180.

Meinhold, G., Kostopoulos, D. K., 2013. The Circum-Rhodope Belt, northern Greece: Age, provenance, and tectonic setting. Tectonophysics 595 - 596, 55 - 68.

Meinhold, G., Kostopoulos, D., Reischmann, T., Frei, D., BouDagher-Fadel, M. K., 2009. Geochemistry, provenance and stratigraphic age of metasedimentary rocks from the eastern Vardar suture zone, northern Greece. Palaeogeography, Palaeoclimatology, Palaeoecology 277, 199 - 225.

Meinhold, G., Kostopoulos, D., Frei, D., Himmerkus, F., Reischmann, T., 2010. U-Pb LASF-ICP-MS zircon geochronology of the Serbo-Macedonian Massif, Greece: palaeotectonic constraints for Gondwana-derived terranes in the Eastern Mediterranean International Journal of Earth Sciences (Geologische Rundschau) 99(4), 813 - 832.

Michailidis, K. M., 1991. Fe-Cr spinel and ilmenite massive mineralization in metamorphic ultramafics from the Askos area, northern Greece. Bulletin of the Geological Society of Greece, XXV(2) 203 - 224.

Michard, A., Goffé, B., Liati, A., Mountrakis, D., 1994. Blueschist-facies assemblages in the peri-Rhodopian zone, and hints for an Eohellenic HP-LT belt in northern Greece. Bulletin of the Geological Society of Greece XXX(1), 185 - 192.

Molnar, P., England, P., 1990. Temperatures, heat flux and frictional stress near major thrust faults. Journal of Geophysical Research 95(B4), 4833 - 4856.

Monod, O., 1964. Étude géologique de massif de Chortiatis (Macédoine grecque), Ph.D. thesis, Université de Paris.

Moulas, E., Kostopoulos, D., Connolly, J. A. D., Burg, J.-P., 2013. P-T Estimates and Timing of the Sapphirine-Bearing Metamorphic Overprint in Kyanite Eclogites from Central Rhodope, Northern Greece. Petrology 21(5), 507 - 521.

Mposkos, E. D., Kostopoulos, D. K., 2001. Diamond, former coesite and supersilicic garnet in metasedimentary rocks from the Greek Rhodope: a new ultrahigh-pressure metamorphic province established. Earth and Planetary Science Letters 192(4), 497 - 506.

Negulescu, E., Săbău, G., Massonne, H.-J., 2009. Chloritoid-Bearing Mineral Assemblages in High-Pressure Metapelites from the Bughea Complex, Leaota Massif (South Carpathians). Journal of Petrology 50(1), 103 - 125.

Okay, A. I., 1989. An Exotic Eclogite/Blueschist Slice in a Barrovian Style Metamorphic Terrain, Alanya Nappes, Southern Turkey. Journal of Petrology 30(1), 107 - 132.

Papadopoulos, C., Kilias, A., 1985. Altersbeziehungen zwischen Metamorphose und Deformation im zentralen Teil des Serbomazedonischen Massivs (Vertiskos Gebirge, NordGriechenland). Geologische Rundschau 74(1), 77 - 85.

Papanikolaou, D., 2009. Timing of tectonic emplacement of the ophiolites and terrane paleogeography in the Hellenides. Lithos 108(1 - 4), 262 - 280.

Papanikolaou, D. J., 2013. Tectonostratigraphic models of the Alpine terranes and subduction history of the Hellenides. Tectonophysics 595 - 596, 1 - 24.

Perraki, M., Proyer, A., Mposkos, E., Kaindl, R., Hoinkes, G., 2006. Raman microspectroscopy on diamond, graphite and other carbon polymorphs from the ultrahighpressure metamorphic Kimi Complex of the Rhodope Metamorphic Province, NE Greece. Earth and Planetary Science Letters 241(3 - 4), 672 - 685.

Powell, R., Holland, T., 1990. Calculated mineral equilibria in the pelite system, KFMASH (K2O-FeO-MgO-Al2O3-SiO2-H2O). American Mineralogist 75, 367 - 380.

Proyer, A., Mposkos, E., Baziotis, I., Hoinkes, G., 2008. Tracing high-pressure metamorphism in marbles: Phase relations in high-grade aluminous calcite-dolomite marbles from the Greek Rhodope massif in the system CaO-MgO-Al2O3-SiO2-CO2 and indications of prior aragonite. Lithos 104(1 - 4), 119 - 130.

Ricou, L.-E., Burg, J.-P., Godfriaux, I., Ivanov, Z., 1998. Rhodope and Vardar: the metamorphic and the olistostromic paired belts related to the Cretaceous subduction under Europe. Geodinamica Acta 11(6), 285 - 309.

Royden, L. H., Papanikolaou, D. J., 2011. Slab segmentation and late Cenozoic disruption of the Hellenic arc. Geochemistry Geophysics Geosystems 12, Q03010.

Sakellariou, D., Dürr, S., 1993. Geological structure of the Serbo-Macedonian massif in NE Chalkidiki peninsula. Bulletin of the Geological Society of Greece XXVIII(1), 179 - 193.

Schmidt, S., Nagel, T. J., Froitzheim, N., 2010. A new occurrence of microdiamond-bearing metamorphic rocks, SW Rhodopes, Greece. European Journal of Mineralogy 22, 189 - 198.

Siivola, J., Schmid, R., 2007. Systematic Nomenclature for Metamorphic Rocks. 12. List of Mineral Abbreviations. Recommendations by the IUGS Subcommission on the Systematics of Metamorphic Rocks. www.bgs.ac.uk/scmr/docs/papers/paper_12.pdf.

Smye, A. J., Greenwood, L. V., Holland, T. J. B., 2010. Garnet-chloritoid-kyanite assemblages: eclogite facies indicators of subduction constraints in orogenic belts. Journal of Metamorphic Geology 28(7), 753 - 768.

Spear, F. S., Cheney, J. T., 1989. A petrogenetic grid for pelitic schists in the system SiO2-Al2O3-FeO-MgO-K2O-H2O. Contributions to Mineralogy and Petrology 101(2), 149 - 164.

Stampfli, G., Borel, G., 2002. A plate tectonic model for the Paleozoic and Mesozoic constrained by dynamic plate boundaries and restored synthetic oceanic isochrons. Earth and Planetary Science Letters 196(1 - 2), 17 - 33.

Symmes, G. H., Ferry, J. M., 1992. The effect of whole-rock MnO content on the stability of garnet in pelitic schists during metamorphism. Journal of Metamorphic Geology 10(2), 221 - 237.

Tajčmanová, L., Connolly, J. A. D., Cesare, B., 2009. A thermodynamic model for titanium and ferric iron solution in biotite. Journal of Metamorphic Geology 27(2), 153 - 165.

Wei, C., Powell, R., 2003. Phase relations in high-pressure metapelites in the system KFMASH (K2O-FeO-MgO-Al2O3-SiO2-H2O) with application to natural rocks. Contributions to Mineralogy and Petrology 145(3), 301 - 315.

White, R. W., Powell, R., N., P. G., 2003. A mineral equilibria study of the hydrothermal alteration in mafic greenschist facies rocks at Kalgoorlie, Western Australia. Journal of Metamorphic Geology 21(5), 455 - 468.

White, R. W., Powell, R., Johnson, T. E., 2014. The effect of Mn on mineral stability in metapelites revisited: new a-x relations for manganese-bearing minerals. Journal of Metamorphic Geology 32(8), 809 - 828.

White, S. H., Powell, R., Holland, T., Worley, B. A., 2000. The effect of TiO2 and Fe2O3 on metapelitic assemblages at greenschist and amphibolite facies conditions: mineral equilibria calculations in the system K2O-FeO-MgO-Al2O3-SiO2H2O-TiO2-Fe2O3. Journal of Metamorphic Geology 18(5), 497 - 511.

Whitney, D., Teyssier, C., Toraman, E., Seaton, N. C. A., Fayon, A. K., 2011. Metamorphic and tectonic evolution of a structurally continuous blueschist-to-Barrovian terrane, Sivrihisar Massif, Turkey. Journal of Metamorphic Geology 29(2), 193 - 212.

FIGURE CAPTIONS

Figure 1. (a) Simplified geological map of the North Aegean after Ricou et al. (1998), Brun and Sokoutis (2007) and Burg (2012). The Vardar Suture Zone separates Pelagonia, to the west, from Rhodopia, to the east. The Rhodope cover a large part of the latter and its two extreme parts are the Northern Rhodope Domain, to the northeast, and the Chalkidiki block, to the southwest. Both parts recorded Mesozoic fabrics and were separated only after Eocene extension and formation of the Southern Rhodope Core Complex (Brun and Sokoutis, 2007) whose timing of development partly overlaps that of the Northern Rhodope Core Complex (see Kydonakis et al., 2015; and references therein) further to the northeast. The study area (Chalkidiki block) is shown in a red rectangle. Cross-section re-drawn after Kydonakis et al. (2015). (b) Geological map of the Chalkidiki block after Kockel and Mollat (1977). Sample localities are shown in orange stars both on the map and on the regional cross-section. The three units of interest are the Vertiskos Unit (basement), the Circum-Rhodope belt (cover) and the Chortiatis Magmatic Suite (arc).

Figure 2. Back-scattered images of sample CR4. (a,b) The microlithons are made of coarse-grained phengite, quartz and chlorite whereas the cleavage domains are made of fine-grained intergrowths of phengite, paragonite, chlorite and quartz. (c) Close view of the cleavage domain. (d) Rare garnet relict that escaped replacement by chlorite. Mineral abbreviation scheme after Siivola and Schmid (2007).

Figure 3. Field occurrences of the studied garnet-staurolite micaschists: (a) Sample SM54, (b) Sample SM40. Garnet appears as porphyroblasts embedded in a matrix made mainly of

white micas and staurolite. Shear bands (dashed lines) are associated with shearing toward the SW (white arrows). Please note also the macroscopically-visible spiral garnet at the centre of the right picture.

Figure 4. Back-scattered images of sample SM54. (a) The internal foliation (S_i) in the garnet is made of elongated chloritoid, paragonite, margarite and rutile rimmed by ilmenite. (b) Fine-grained intergrowths of phengite and paragonite from the matrix. (c,d) The internal foliation (S_i) in the staurolite contains quartz, rutile (often replaced by ilmenite) and biotite.

Figure 5. Mineral chemistry of the white micas for the three studied samples. (left) Tschermak substitution [$Al_2Si_{-1}(FeMg)_{-1}$] compositional trend and (right) $Al^{(total)}$ vs Na/(Na+K) plot.

Figure 6. Garnet chemistry for the three studied samples. For sample CR4 garnet is heavily replaced by chlorite and thus, the acquired analyses is ambiguous whether they represent core or rim compositions. For samples SM54 and SM40 a clear compositional trend exists from core to rim.

Figure 7. Representative garnet Ca, Fe, Mg and Mn element maps (left) and microprobe elemental profiles (right) for sample SM54. Colour code in the elemental maps corresponds to counts per second (cps) (warm-redish colours – maximum cps; cool-bluish colours –

minimum cps). The profile corresponds to red dashed line superimposed on the Ca compositional map.

Figure 8. (left) Isochemical phase-diagram section for sample CR4. Colour code for field variance (darker colour for higher variance fields). (right) Selected compositional isopleths for garnet, phengite and chlorite are superimposed on the section. Inferred P-T conditions are shown in pale grey. See text for details.

Figure 9. (left) Isochemical phase-diagram section for sample SM54. Colour code for field variance (darker colour for higher variance fields). (right) Selected compositional isopleths for garnet, chloritoid, phengite, staurolite and biotite are superimposed on the section. Inferred P-T conditions are shown in pale grey based on 1: Garnet core composition, chloritoid composition (as inclusion in garnet) and the maximum silica content of the phengite, 2: Garnet rim composition, 3: Kyanite and biotite composition (as inclusion in staurolite) and 4: Staurolite composition. The related metamorphic path is drawn. See text for details.

Figure 10. Compilation of representative P-T estimates for the Chalkidiki block (light grey) and the central/western Northern Rhodope Domain (dark grey). M94: Michard et al. (1994), K91: Kourou (1991), K99: Kilias et al. (1999), M91 Michailidis (1991), DK: Dimitrios Kostopoulos, pers. comm. 2014, LS96: Liati and Seidel (1996), K10: Krenn et al. (2010), M13: Moulas et al. (2013), KM02: Krohe and Mposkos (2002). See text for details.

Appendix A1. Mineral compositional contours and mineral isomodes for sample CR4.

Appendix A2. (left) Isochemical phase-diagram section for sample SM40. Colour code for field variance (darker colour for higher variance fields). (right) Selected compositional isopleths for garnet, phengite and chlorite are superimposed on the section. The inferred P-T conditions (pale grey areas) and related metamorphic path are shown based on 1: Garnet core composition, chlorite composition (as inclusion in garnet) and the maximum silica content of the phengite, 2: Garnet rim composition, 3: Existence of staurolite (in the absence of kyanite) and 4: Matrix chlorite composition.

Appendix A3. Mineral compositional contours and mineral isomodes for sample SM40.

Appendix A4. Representative garnet Ca, Fe, Mg and Mn element maps (left) and microprobe elemental profiles (right) for sample SM40. Colour code in the elemental maps corresponds to counts per second (cps) (warm colours – maximum cps; cool colours – minimum cps). The profile corresponds to red dashed line superimposed on the Ca compositional map.

Appendix A5. Mineral compositional contours and mineral isomodes for sample SM54.

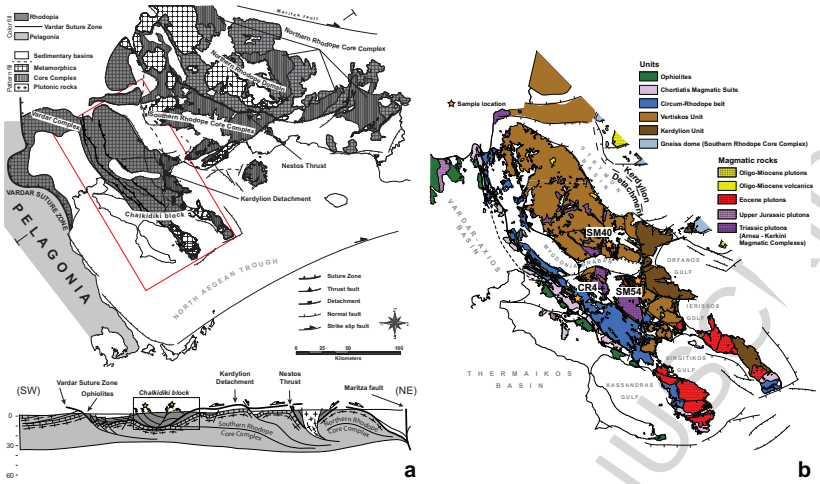

Figure 1

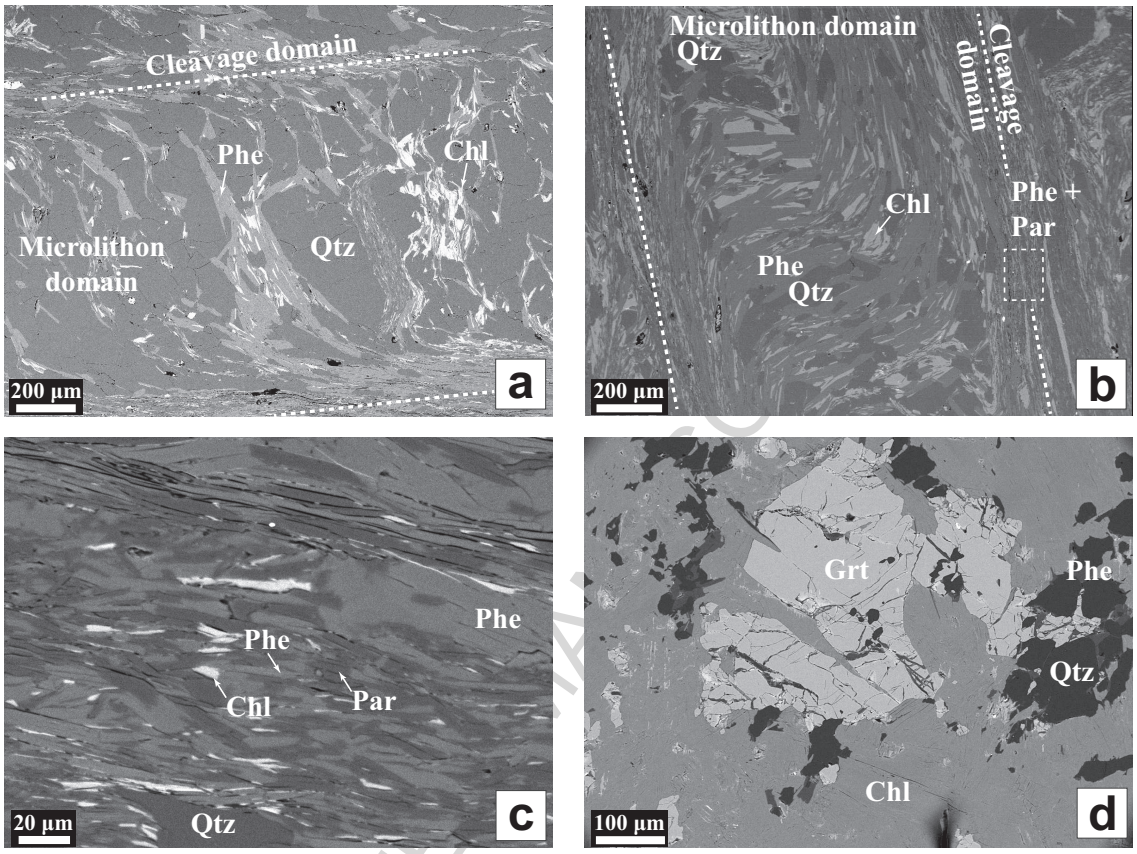

Figure 2

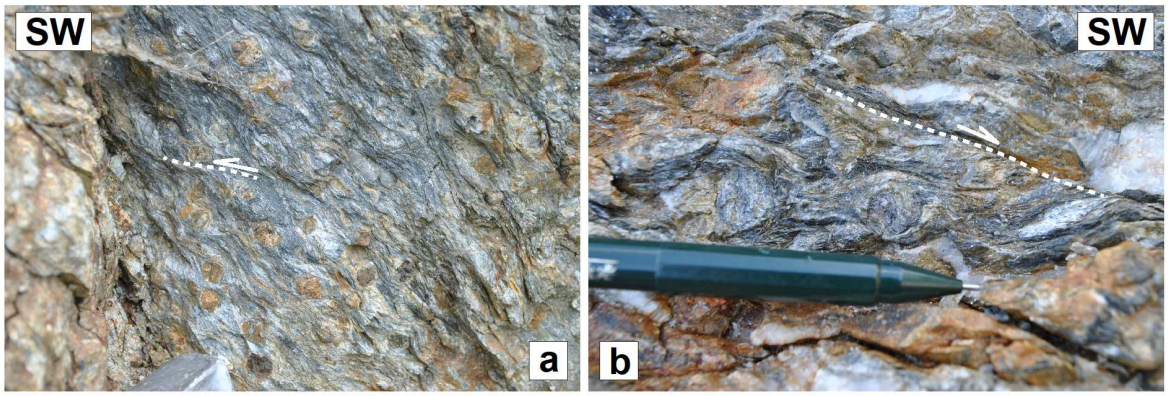

Figure 3

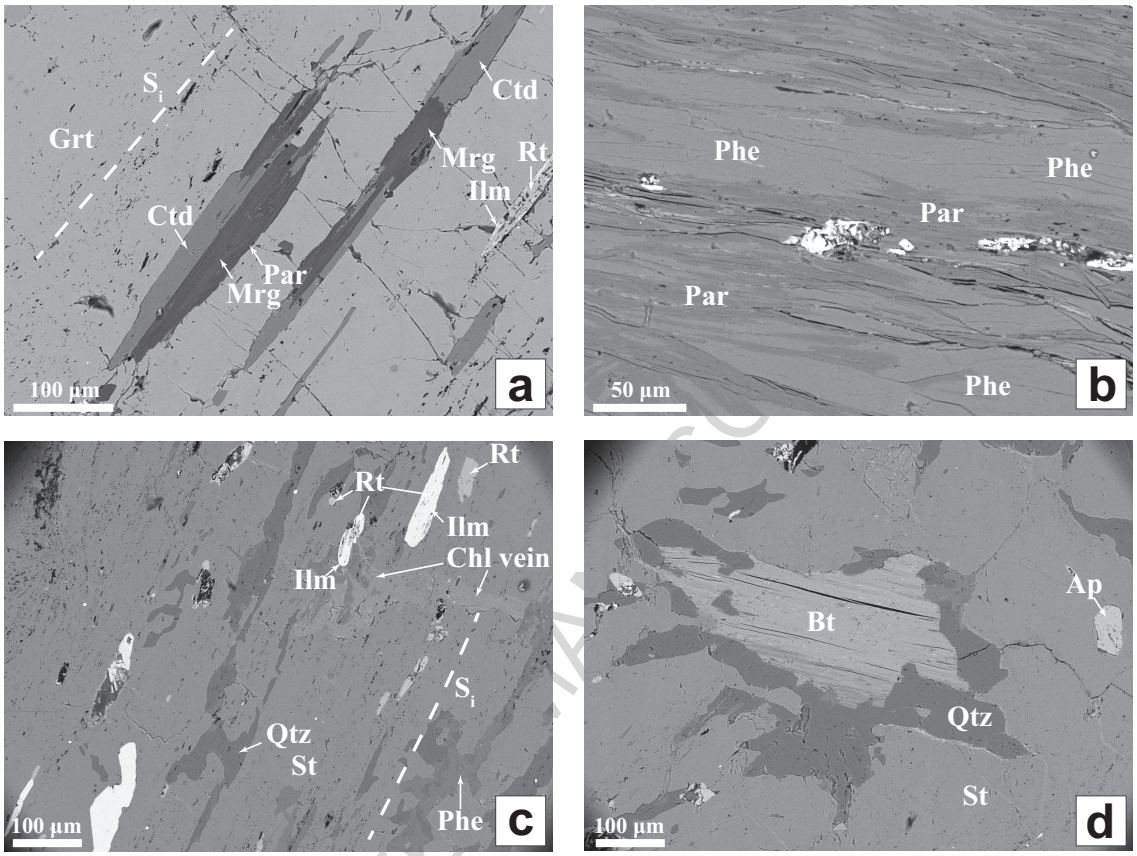

Figure 4

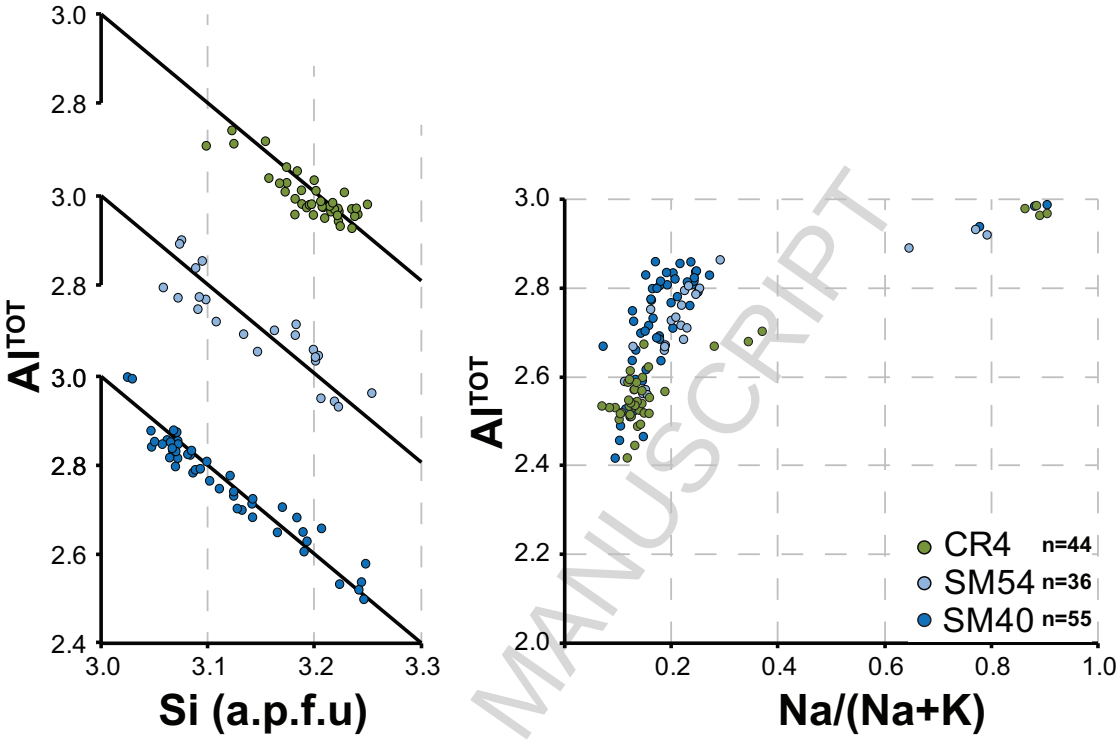

Figure 5

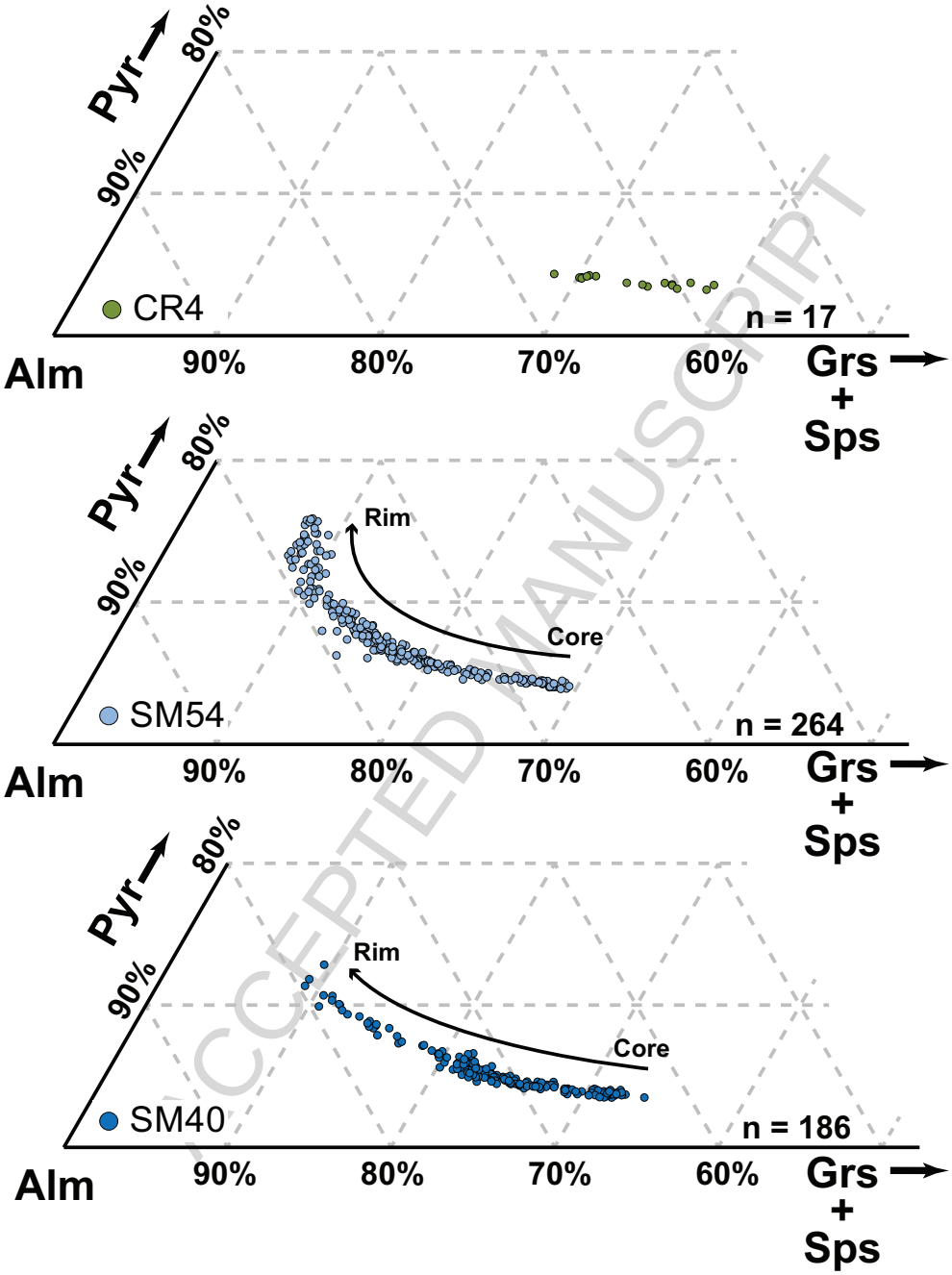

Figure 6

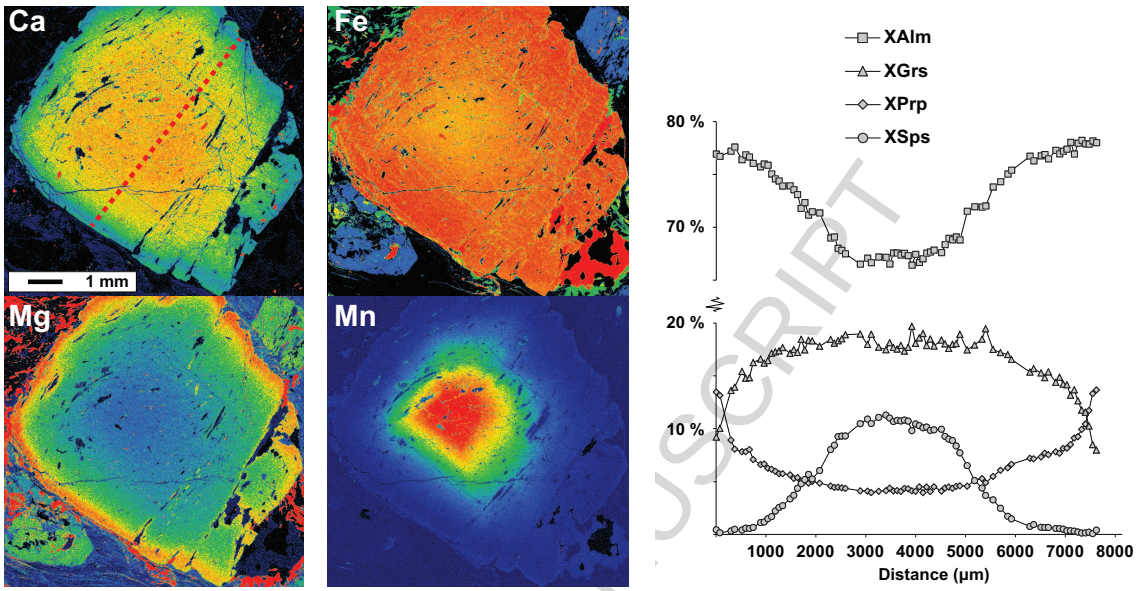

Figure 7

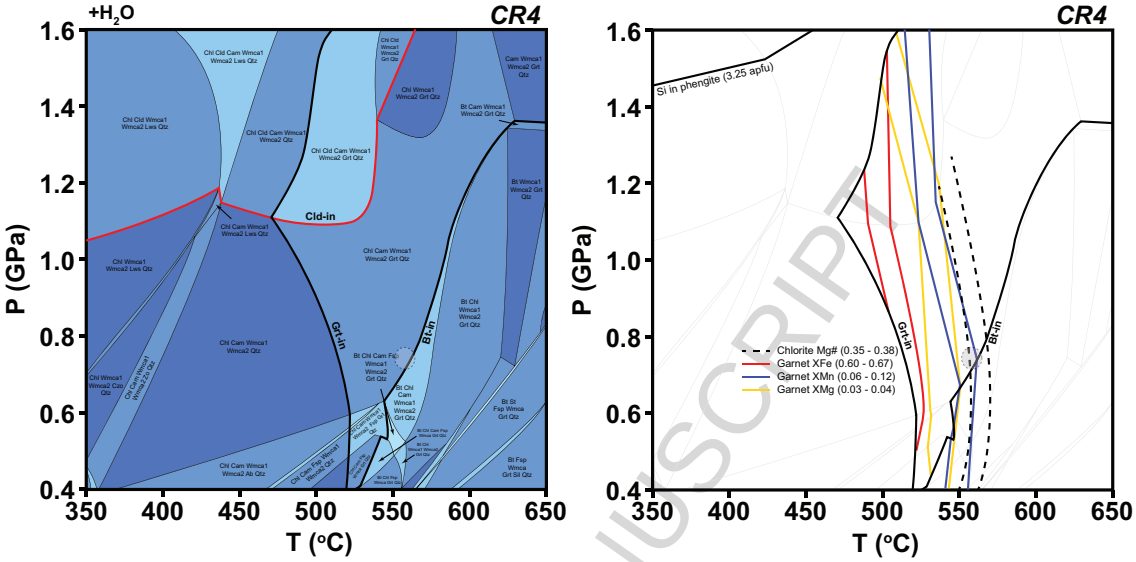

Figure 8

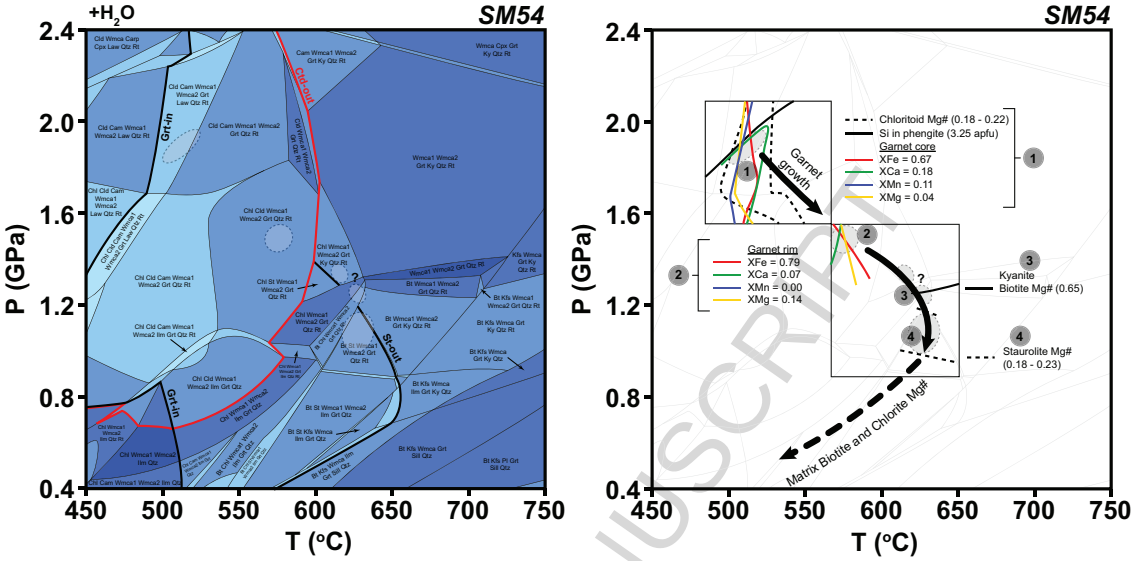

Figure 9

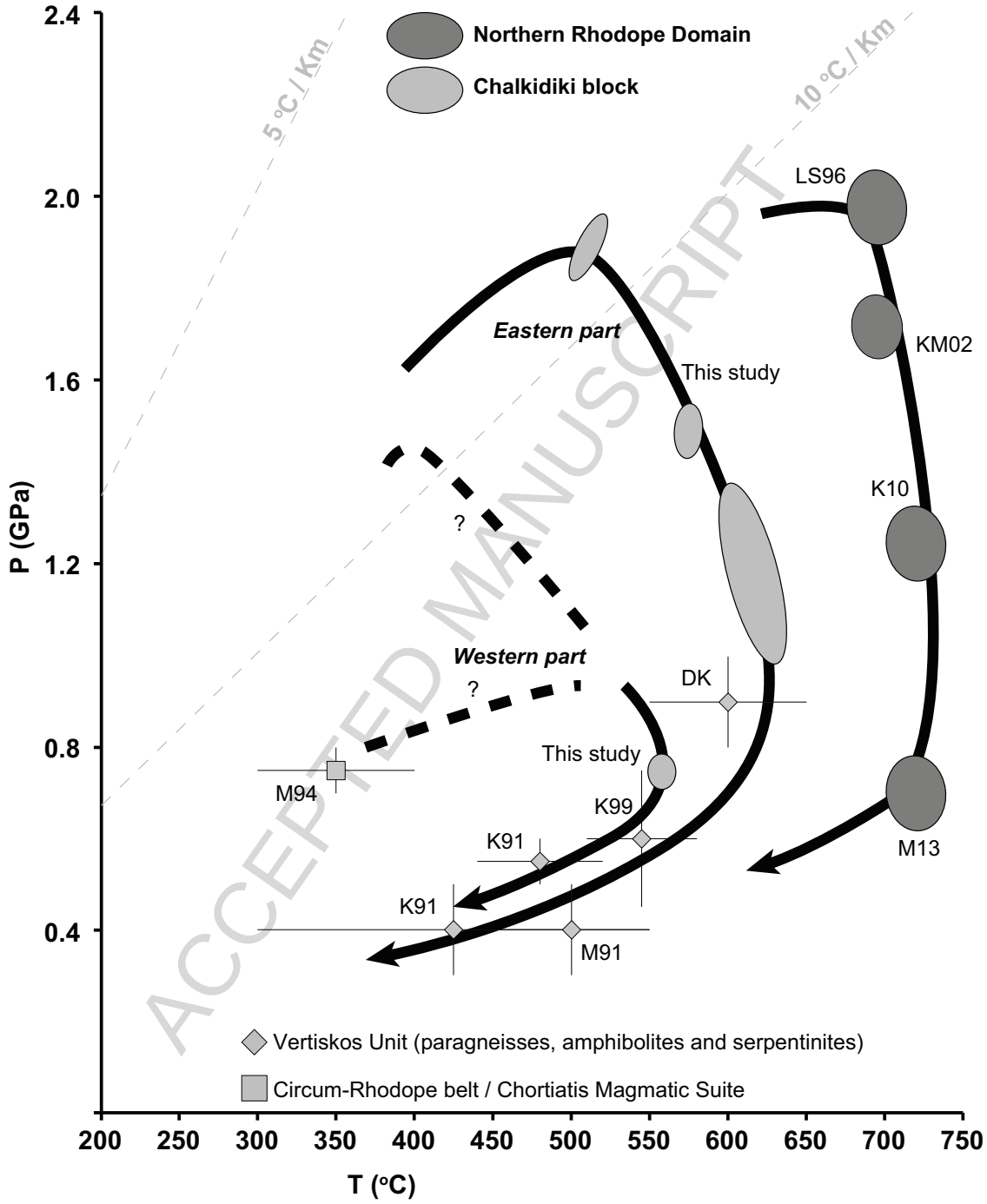

Figure 10

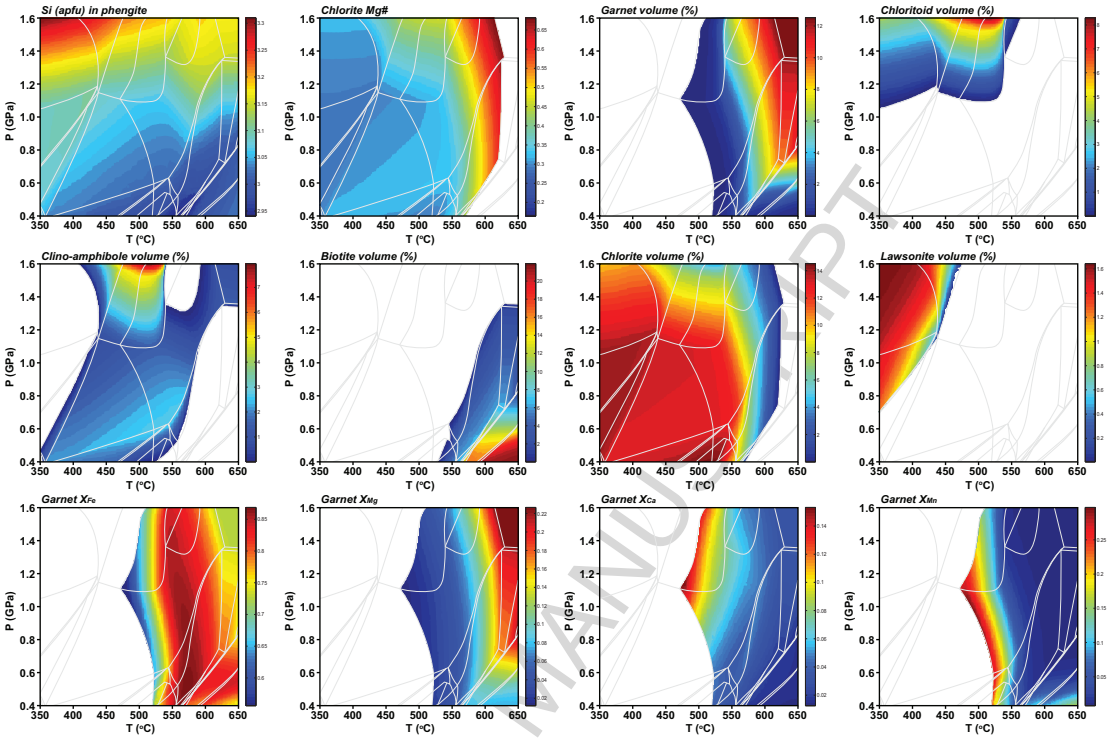

Appendix A1

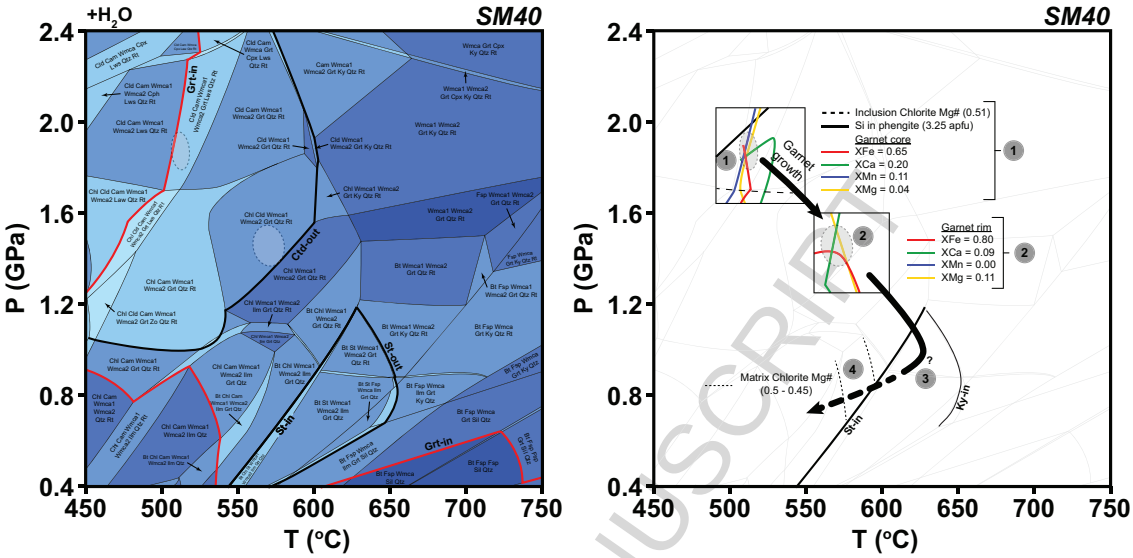

Appendix A2

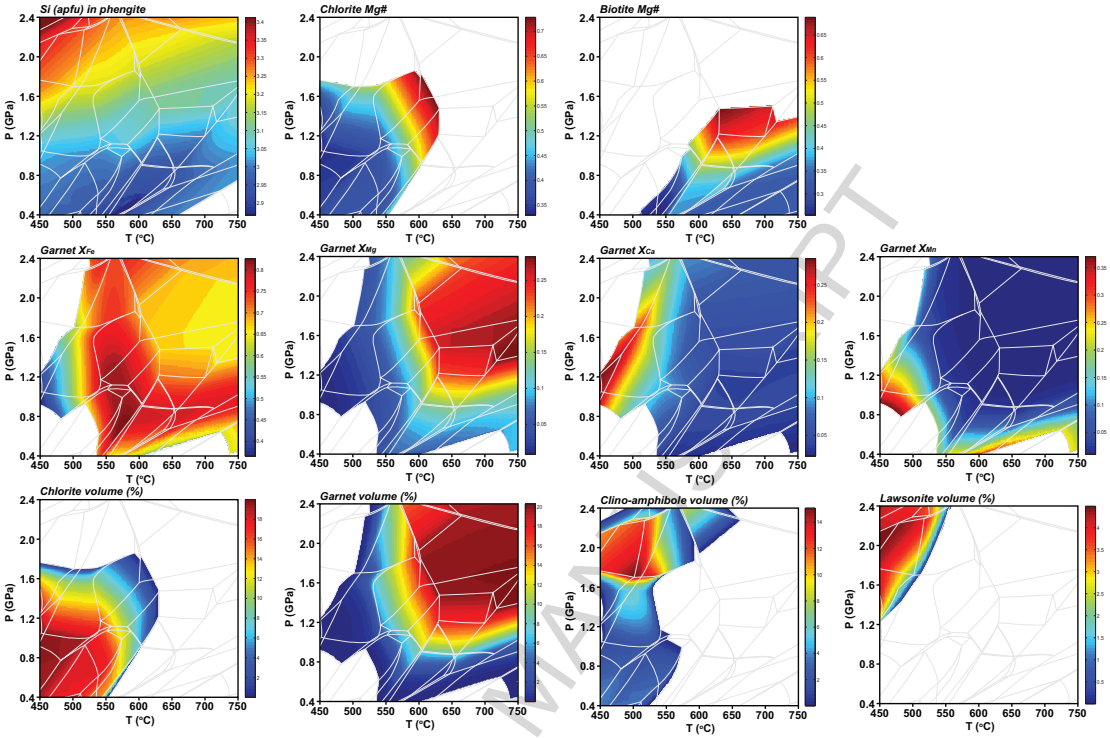

Appendix A3

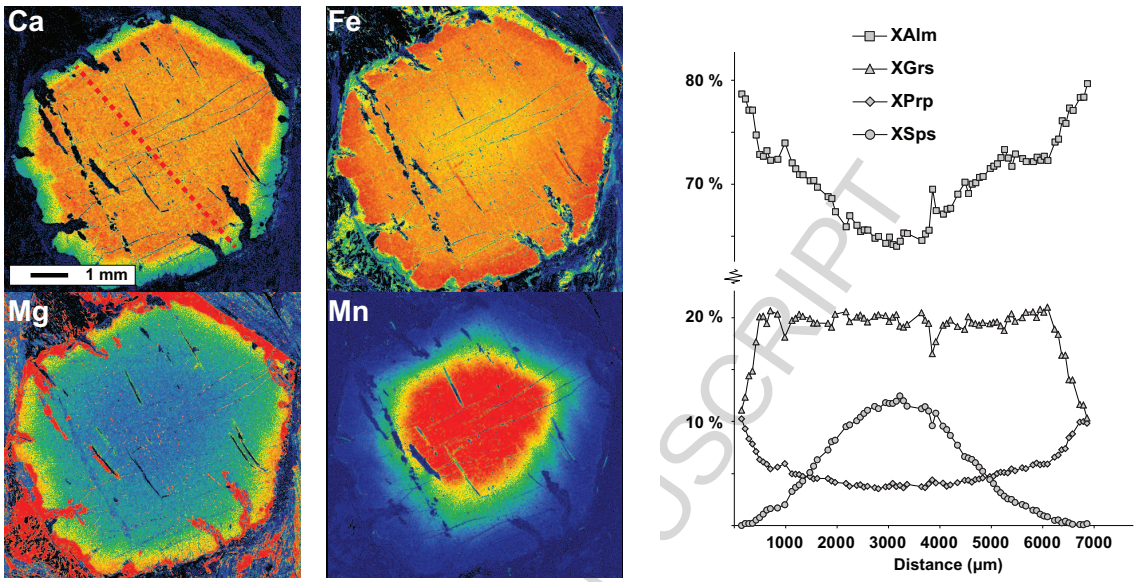

Appendix A4

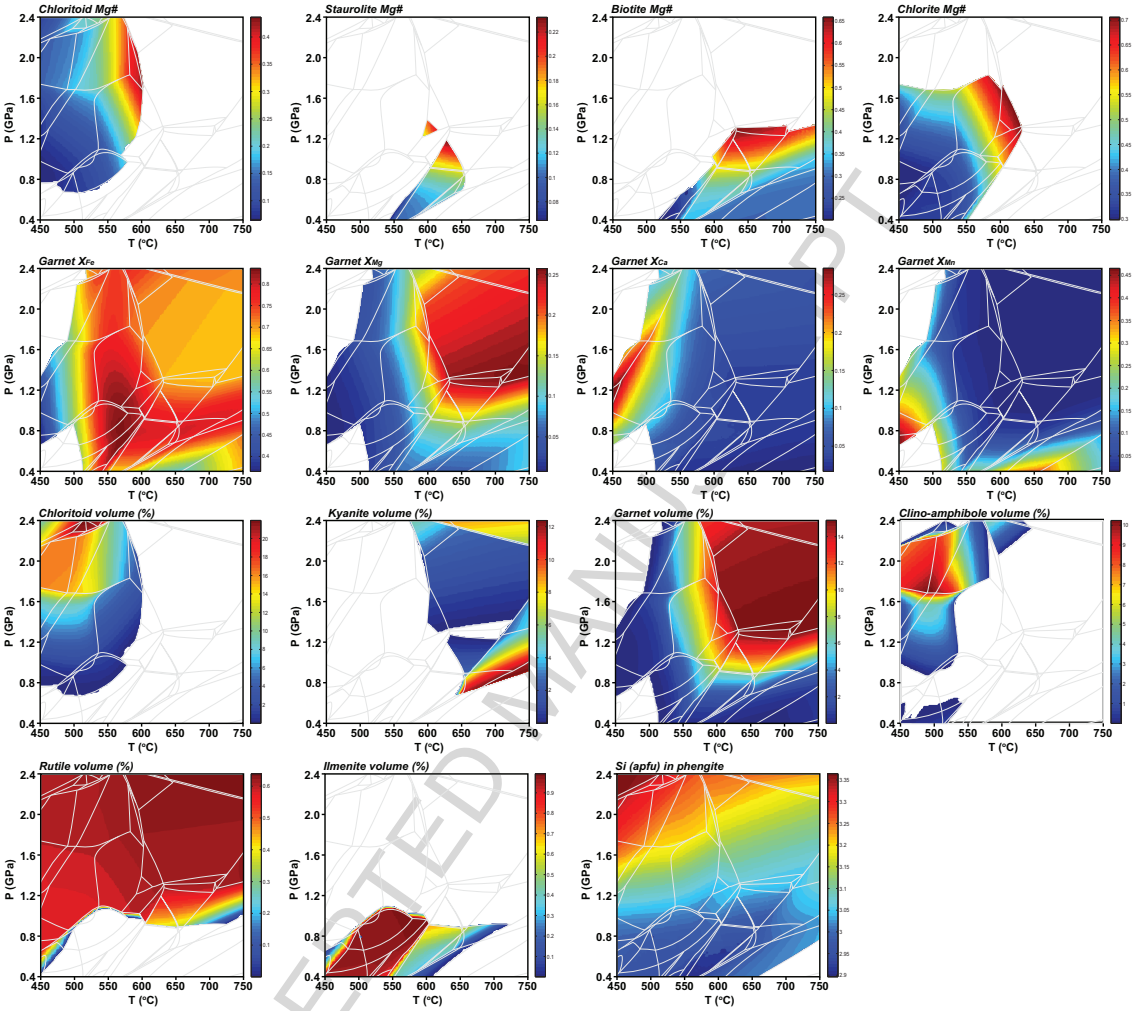

Appendix A5

Table 1. Solid solution models used for the phase-diagram sections.

Mineral / Phase	Solution Model	Source
Biotite	Bio(TCC)	Tajčmanová et al. (2009)
Feldspars	feldspar	Fuhrman and Lindsley (1988)
Garnet	Gt(GCT)	Ganguly et al. (1996)
Ilmenite	IlGkPy	Ideal
White Mica	Mica(CHA1)	Auzanneau et al. (2010); Coggon and Holland (2002)
Chlorite	Chl(HP)	Holland et al. (1998)
Staurolite	St(HP)	parameters from THERMOCALC
Chloritoid	Ctd(HP)	White et al. (2000)
Clino-amphibole	GlTrTsPg	Wei and Powell (2003); White et al. (2003)
Clino-pyroxene	Omph(GHP2)	Diener and Powell (2012)

Table 2. Mineralogical assemblage table and corresponding bulk rock compositions of the studied samples.

	Sample	*CR4*		*SM40*		*SM54*	
	Latitude	40.526	modal	40.761	modal	40.610	modal
	Longitude	23.222	%	23.415	%	23.603	%
	Rocktype	*garnet phyllite*		*garnet-staurolite-mica schist*			
Major phases	**quartz**	x	*40*	x	*15*	x	*15-20*
	muscovite	x	*25-30*	x	*40*	x	*30-35*
	paragonite	x	*10-15*	x	*10-15*	x	*10*
	margarite					*	*<5*
	chloritoid					*	*<5*
	biotite			chloritised	*5*	x	
	garnet	x	*10*	x	*10-15*	x	*10*
	kyanite					x	*<5*
	staurolite			x	*5*	x	*5*
	chlorite	x	*10-15*	x	*10*	x	*15*
Accesory phases	**rutile**			x		x	
	ilmenite			x		x	
	monazite			x			
	apatite					x	
	zircon	x		x		x	
	allanite			x			
	fe-oxides	x				x	
Whole rock chemistry							
	SiO_2	63.67		44.46		56.12	
	TiO_2	0.57		1.15		0.82	
	Al_2O_3	16.60		27.65		21.77	
	Fe_2O_3	4.24		3.00		3.18	
	FeO	2.11		5.32		3.61	
	MnO	0.06		0.12		0.14	
	MgO	1.44		2.26		1.56	
	CaO	0.31		0.85		0.80	
	Na_2O	1.04		1.55		1.34	
	K_2O	2.81		4.68		3.32	
	P_2O_5	0.17		0.16		0.19	
	LOI	5.30		7.06		5.46	
	Total	98.32		98.25		98.32	

* Only as inclusion

Table3. Representative electron microprobe mineral analyses (in wt %).

sample	*CR4*	*CR4*	*CR4*	*CR4*	*CR4*	*CR4*	*SM54*	*SM54*	*SM54*	*SM54*	*SM54*	*SM54*	*SM54*	*SM54*	*SM54*	*SM54*	*SM54*	*SM54*	*SM54*	*SM54*	*SM54*	*SM40*	*SM40*	*SM40*	*SM40*	*SM40*	*SM40*	*SM40*	*SM40*	*SM40*
rock type	*phyllite*	*phyllite*	*phyllite*	*phyllite*	*phyllite*	*phyllite*	*grt-stsc hist*	*grt-stsc hist*	*grt-stsc hist*	*grt-stsc hist*	*grt-stsc hist*	*grt-stsc hist*	*grt-stsc hist*	*grt-stsc hist*	*grt-stsc hist*	*grt-stsc hist*	*grt-stsc hist*	*grt-stsc hist*	*grt-stsc hist*	*grt-stsc hist*	*grt-stsc hist*	*grt-stsc hist*	*grt-stsc hist*	*grt-stsc hist*	*grt-stsc hist*	*grt-stsc hist*	*grt-stsc hist*	*grt-stsc hist*	*grt-stsc hist*	*grt-stsc hist*
mineral	chl	phe	phe	par	grt	grt	chl	chl	bt	ctd	ctd	par	par	mrg	ms	phe	st	st	grt	grt	grt	grt	chl	chl	par	phe	phe	ms	grt	grt	grt	grt
texture	replaced by chl	matrix	matrix	matrix	replaced by chl	replaced by chl	matrix	inclusion (st)	inclusion (st)	inclusion (grt)	inclusion (grt)	matrix	inclusion (grt)	inclusion (grt)	matrix	matrix	matrix	matrix	rim	rim	core	core	matrix	inclusion (grt)	matrix	matrix	matrix	matrix	rim	rim	core	core
SiO_2	24.53	47.07	48.91	46.66	37.24	37.12	29.52	26.85	38.40	25.32	24.96	45.66	43.35	29.81	46.65	48.75	28.99	28.40	37.79	37.78	37.43	37.17	24.87	25.25	46.16	49.14	48.57	46.09	37.21	37.19	36.72	37.08
TiO_2	0.02	0.37	-	0.05	0.09	0.14	2.54	-	1.39	-	-	-	-	-	0.44	-	0.48	0.55	0.05	0.08	0.07	0.12	0.09	0.35	-	-	-	-	0.05	-	0.09	0.17
Al_2O	21.7	32.	32.	39.	21.3	21.2	20.	22.6	21.3	41.1	41.0	40.	41.7	50.6	35.	32.	54.	54.	21.	21.	21.	21.	22.	22.6	40.	31.	31.	36.	21.	21.	21.	20.

$_3$	8	87	23	91	2	3	352	0	9	3	3	69	4	1	37	85	661	081	403	563	453	243	562	0	19	97	91	35	043	143	062	992
FeO(T)	30.19	2.10	2.32	0.78	30.34	28.37	27.01	20.83	12.54	22.52	23.43	-	1.05	1.10	1.08	1.17	13.10	2.87	35.95	35.18	30.05	30.14	28.23	26.01	0.59	1.47	1.63	1.15	35.48	35.23	29.05	29.17
MnO	0.43	0.03	-	0.02	2.50	5.27	0.03	-	-	-	-	-	-	-	-	-	0.02	0.02	0.18	0.06	4.90	4.83	0.08	-	-	-	-	-	0.08	0.04	4.98	4.82
MgO	10.57	1.46	1.68	0.11	1.10	0.92	8.09	17.21	13.30	3.52	2.98	-	-	-	0.97	1.70	1.62	2.19	3.53	3.38	1.10	1.03	12.86	14.38	-	2.14	1.83	0.76	2.67	2.51	0.94	0.89
CaO	0.01	-	-	0.25	7.92	7.87	0.30	-	-	-	-	0.88	1.89	12.22	-	-	0.01	-	2.86	3.58	6.38	6.29	0.05	-	0.76	-	-	-	3.59	4.09	7.18	6.99
Na_2O	-	1.09	0.88	6.54	0.01	0.03	0.11	-	-	-	-	6.80	6.57	1.27	1.63	1.17	-	-	0.02	-	-	0.04	-	-	6.61	0.79	0.91	1.52	0.06	0.14	0.01	0.04
K_2O	-	9.72	9.56	1.09	0.01	-	0.80	-	8.64	-	-	1.17	0.60	0.00	8.85	9.74	-	-	-	-	-	-	0.05	-	1.39	10.27	9.91	9.78	0.02	0.04	-	-
TOTAL	**87.52**	**94.70**	**95.58**	**95.41**	**100.53**	**100.97**	**88.78**	**87.50**	**98.10**	**92.49**	**92.40**	**95.19**	**95.20**	**95.01**	**95.00**	**95.38**	**98.90**	**98.13**	**1017.78**	**1016.62**	**1013.38**	**1008.86**	**8881**	**88.60**	**95.70**	**95.78**	**94.76**	**95.65**	**1000.22**	**1000.37**	**1000.04**	**1000.14**
	[14]O	[11]O	[11]O	[11]O	[12]O	[12]O	[14]O	[14]O	[11]O	[12]O	[12]O	[11]O	[11]O	[11]O	[11]O	[11]O	[23]O	[23]O	[12]O	[12]O	[12]O	[12]O	[14]O	[14]O	[11]O	[11]O	[11]O	[11]O	[12]O	[12]O	[12]O	[12]O

Si	2.66	3.16	3.24	2.98	2.98	2.97	3.07	2.75	2.77	2.06	2.04	2.93	2.80	2.00	3.09	3.22	3.95	3.90	2.98	2.98	2.98	2.98	2.62	2.63	2.95	3.25	3.24	3.05	2.99	2.98	2.97	2.99
Ti	0.00	0.02	-	0.00	0.01	0.01	0.20	-	0.08	-	-	-	-	-	0.02	'-	0.05	0.06	0.00	0.00	0.00	0.01	0.01	0.03	-	-	-	-	0.00	-	0.01	0.01
Al	2.79	2.60	2.51	3.01	2.01	2.00	2.50	2.73	1.82	3.95	3.96	3.08	3.18	3.99	2.76	2.56	8.78	8.76	1.99	2.00	2.01	2.01	2.80	2.78	3.03	2.49	2.51	2.83	1.99	2.00	2.01	1.99
Fe +2	2.74	0.12	0.13	0.04	2.03	1.90	2.35	1.78	0.76	1.53	1.61	-	0.06	0.06	0.06	0.06	1.49	1.48	2.37	2.32	2.00	2.02	2.49	2.27	0.03	0.08	0.09	0.06	2.38	2.36	1.96	1.97
Mn	0.04	0.00	-	0.00	0.17	0.36	0.00	-	-	-	-	-	-	'-	-	-	0.00	0.00	0.01	0.00	0.33	0.33	0.01	-	-	-	-	-	0.01	0.00	0.34	0.33
Mg	1.71	0.15	0.17	0.01	0.13	0.11	1.26	2.63	1.43	0.43	0.36	-	-	-	0.10	0.17	0.33	0.45	0.42	0.40	0.13	0.12	2.02	2.24	-	0.21	0.18	0.07	0.32	0.30	0.11	0.11
Ca	0.00	0.00	-	0.02	0.68	0.67	0.03	-	-	-	-	-	0.13	0.88	-	-	0.00	-	0.24	0.30	0.54	0.54	0.01	-	0.05	-	-	'-	0.31	0.35	0.62	0.60
Na	0.00	0.14	0.11	0.81	0.00	0.00	0.02	-	-	-	-	0.85	0.82	0.17	0.21	0.15	-	-	0.00	-	-	0.01	-	-	0.82	0.10	0.12	0.19	0.01	0.02	0.00	0.01
K	0.00	0.83	0.81	0.09	0.00	-	0.11	-	0.79	-	-	0.10	0.05	0.00	0.75	0.82	-	-	-	-	-	-	0.01	-	0.11	0.87	0.84	0.83	0.00	0.00	-	-
TOTAL	9.94	7.01	6.97	6.96	8.01	8.02	9.54	9.89	7.64	7.97	7.97	7.00	7.04	7.09	6.99	6.98	14.61	14.66	8.02	8.01	8.01	8.01	9.97	9.95	7.00	6.99	6.98	7.04	8.02	8.03	8.02	8.01
Mg#	*0.38*	*0.55*	*0.56*	*0.19*	*0.06*	*0.05*	*0.35*	*0.60*	*0.65*	*0.22*	*0.18*	*0.00*	*0.00*	*0.00*	*0.61*	*0.72*	*0.18*	*0.23*	*0.15*	*0.15*	*0.06*	*0.06*	*0.45*	*0.50*	*0.00*	*0.72*	*0.67*	*0.54*	*0.12*	*0.11*	*0.05*	*0.05*